SAPIENZA
UNIVERSITÀ DI ROMA

Innovative approaches to study exosome biogenesis and uptake: insights into Mannose Receptor-Mediated uptake and immunomodulatory effects on Dendritic Cells

PhD in CELL AND DEVELOPMENTAL BIOLOGY

Department BIOLOGY AND BIOTECHNOLOGIES C. DARWIN

XXXVI cycle

Candidate: Valeria Barreca

PhD Supervisor

Maria Luisa Fiani

PhD tutor

Giancarlo Poiana

A.A. 2022-2023

Index

Synposis

In recent years, exosomes have gained significant attention due to their role in cell-to-cell communication and their potential clinical applications. However, challenges in accurately isolating exosomes from other types of Extracellular Vesicles (EVs) have hindered both their functional studies and clinical utility. Moreover, many aspects related to exosome biogenesis, interaction with recipient cells, and selective uptake mechanisms remain poorly understood. This PhD thesis addresses these challenges and shed light on exosome uptake mechanisms and immunomodulatory effects on immune cells. To develop an effective strategy for labeling exosomes and distinguishing them from microvesicles or ectosomes, we developed an innovative methodology that allows to obtain metabolically labels sEV by using a fluorescent lipid, BODIPY FL C16, which is readily internalized by cells and is transformed into phospholipids, which will form part of the lipid bilayer of the secreted vesicles. Confocal microscopy showed colocalization of BODIPY lipids with lipid transformation sites such as ER and mitochondria and with specific markers of multivesicular bodies (MVB) or other organelles (tetraspanins, Golgi markers, lysosomes). Secretion of fluorescent Bodipy sEV is followed over time and shows an early release into the extracellular medium. The ratio of Bodipy sEV to the total secreted sEV, as determined by Nanoparticle Tracking Analysis (NTA), remains constant for up to 6 hours. Bodipy sEV have been sorted by Fluorescence Activated Cell Sorting (FACS) and analysed by electron microscopy. Results show that sorted Bodipy sEV have the typical shape and size of a subpopulation of sEV often referred to as small exosomes (Exo-S) whereas total sEV were more hetereogenous.

In the second part of this thesis we investigated the mechanisms of exosomes internalization by antigen-presenting cells, specifically immature dendritic cells (iDCs) expressing the mannose receptor (MR/CD206) on their surface. It has been described that exosomes are enriched in high mannose glycans, and since the glycosylation profiles of both cells and exosomes can be altered in hypoxic

conditions, such as those found in the tumor microenvironment (Ryan P. McNamara, 2021), we evaluated the specific uptake mediated by the MR of exosomes secreted under normoxic or hypoxic condition. Our findings revealed that the MR plays a crucial role in the selective uptake of exosomes, as evidenced by the significant decrease of uptake in the presence of yeast mannan (y.mannan), a MR competitive binding inhibitor. Both normoxic and hypoxic exosomes are as effective as LPS to induce DC maturation, as evidenced by the increased expression of CD80, CD86 and CD83, but only normoxic exosomes downregulate the MR/CD206. This data suggest the potential role of exosomes in modulating immune responses in the tumor microenvironment. Furthermore, preliminary data suggested that exosomes may contribute to immune modulation, as evidenced by the increased secretion of TNF-α and IL-12p70 by DCs treated with normoxic exosomes. Future investigations will delve into the cytokine secretion profiles of exosome-treated iDCs and miRNA profiles of normoxic and hypoxic exosomes.

In conclusion, in this thesis is presented an innovative approach for studying exosomes biogenesis and labeling a specific subpopulation. It was demonstrated that exosomes are specifically internalized by the Mannose Receptor expressed on immature dendritic cells (iDCs), and the immunomodulatory potential of exosomes on dendritic cells was highlighted.

1 Introduction

1.1 Extracellular vesicles

Almost all cell types secrete a heterogeneous population of lipid bilayer vesicles, collectively called extracellular vesicles (EVs) (Kalluri & LeBleu, 2020; Teng & Fussenegger, 2020; van Niel, D'Angelo, & Raposo, 2018). Extracellular vesicles (EVs) are principally classified into three groups based on their size and biogenesis: exosomes (30–150 nm), microvesicles (MVs) (100–1000 nm) and apoptotic bodies (> 1000 nm) (Gurung, Perocheau, Touramanidou, & Baruteau, 2021). Apoptotic bodies are released by dying cells and, under certain conditions, they can present different size, structure and composition. In fact, they contain a wide variety of cellular components, including micronuclei, chromatin remnants, cytosolic portions, degraded proteins, DNA fragments, and even intact organelles (Battistelli & Falcieri, 2020). MVs are formed by direct outward budding of the plasma membrane (Clancy, Schmidtmann, & D'Souza-Schorey, 2021; Meldolesi, 2022), whereas exosomes are formed within late endocytic compartments or multivesicular bodies (MVBs) by invagination of the limiting membrane into the lumen. Exosomes are vesicles formed by the introflexion of the membrane of MVBs, leading to the generation of intraluminal vesicles (ILVs). Upon early or late endosomal maturation, MVBs can fuse with the plasma membrane releasing the enclosed intraluminal vesicles in the extracellular space. The fate of MVBs can be different, in fact they can fuse with lysosomes to degrade their cargo or with the plasma membrane to release intraluminal vesicles. Once released into the extracellular environment, MVB-derived intraluminal vesicles are known as exosomes. The biogenesis of intraluminal vesicles can occur through different mechanisms, and more than one mechanism coexists within the same MVB (Colombo, Raposo, & Thery, 2014). Indeed, inhibition of a single pathway does not completely suppress extracellular vesicle biogenesis and release, thus demonstrating that more than one mechanism is active simultaneously within a specific cell type (Aheget et al., 2020; Mathieu, Martin-

Jaular, Lavieu, & Thery, 2019). Genetic EV labeling, which involves tagging EV with fluorescent reporter proteins, has proven to be a very promising technique as it targets known EV markers such as tetraspanins. This technique has several advantages over non-specific labeling techniques, such as PKH26 or carboxyfluorescein diacetate succinimidyl ester (CFDA-SE), and allows for the analysis and characterization of EV at the single-vesicle level. However, tetraspanins, such as CD63, CD9, and CD81, have been identified in some EV subpopulations in different combinations (Kowal et al., 2016).

1.2 Tumor microenvironment

Cancer cells are cells that constantly change their characteristic inducing the generation of abnormal tissue and tumor growth. Solid tumors develop within a complex tumor microenvironment consisting of both cellular and non-cellular elements that often lead to an immunosuppressive behavior (Boussadia et al., 2018; Kalra, Drummen, & Mathivanan, 2016). The TME is a constantly evolving environment in which coexist not only tumor cells, but also endothelial cells, involved in the phenomenon of angiogenesis as they allow the tumor to receive oxygen and nutrients, fibroblasts and cells of the immune system including macrophages, dendritic cells, lymphocytes but also signalling molecules (cytokines and chemokines) and extracellular matrix (Arneth, 2019; Fiani et al., 2020; Nyberg, Salo, & Kalluri, 2008). Dendritic cells (DCs) and tumor-associated macrophages (TAMs) are key players in the TME. DCs are the most potent professional antigen-presenting cells (APCs) and play a critical role in the initiation and regulation of the immune response by presenting antigens to T cells. For the antigen presentation and T cell activation it is important that there is the interaction between receptors and costimulatory molecules capable of activating an immune response. Once activated, dendritic cells release a series of cytokines and chemokines capable of influencing the TME. Other cells that play an important role in the TME are the Tumor Associated Macrophages (TAMs) that can be distinguished into M1 and M2-like macrophages (Khan et al., 2023; Mantovani & Allavena, 2015; Mantovani, Marchesi,

Malesci, Laghi, & Allavena, 2017; Whiteside, 2016; Zou, 2005). M1 macrophages (M1 Φ) have pro-inflammatory and immunostimulatory properties, while M2 macrophages (M2 Φ) provide support for tumor progression, angiogenesis, and metastasis (Laoui et al., 2011; Wanderley et al., 2018).

1.3 Exosomes and their role in cell communication

Tumor cells secrete higher levels of exosomes than non-tumoral cells, which can transfer in oncogenic cargo, including proteins like tetraspanins (CD9, CD63, CD81, and CD82), epithelial cell adhesion molecules (EpCAM) and heat shock proteins (HSP70, HSP90), as well as nucleic acids, in particular many types of RNAs including mRNA, transfer RNAs (tRNAs), viral RNA, and noncoding RNAs such as microRNA (miRNAs) and lncRNAs. These cargo molecules are transmitted to recipient cells and alter their behavior thus promoting cancer cell survival and growth (Han et al., 2017; Kalluri, 2016; Khan et al., 2023; Nail, Chiu, Leung, Ahmed, & Wang, 2023).

Exosomes are key players in cell communication and in the modulation of the Tumor Microenvironment. They can promote tumor progression by inducing epithelial-to-mesenchymal transition (EMT) and enhancing the invasive ability and metastatic potential of cancer cells (Chang, Chiu, Wu, & Shen, 2022; Lucchetti et al., 2020). Exosomes can also promote angiogenesis by carrying pro-angiogenic factors, such as VEGF, FGF to endothelial cells leading to the formation of new blood vessels that provide nutrients and oxygen to the tumor, thereby promoting its growth. Furthermore, they can contribute to drug resistance by transferring drug-resistant molecules to cancer cells, promoting the survival of cancer stem cells, and modulating the expression of drug targets in cancer cells. Overall, exosomes have a diverse range of functions in the TME and understanding their specific roles can provide insights into the development of targeted therapies that disrupt exosomes-mediated tumor progression (Hu et al., 2018; Li & Nabet, 2019; Meckes et al., 2013; Mori et al., 2008; Paskeh et al., 2022; Whiteside, 2016).

1.4 Mechanisms of internalization

Exosomes play a crucial role in intercellular communication under both normal and pathological conditions (Mathieu et al., 2021). Exosomes can be internalized by recipient cells through various mechanisms and once internalized, they can deliver their cargo, including proteins, nucleic acids, and lipids, to the recipient cells and modulate their biological functions. Membrane fusion is one of the mechanisms of exosomes uptake, involving the fusion of the exosomes' membrane with the plasma membrane of the recipient cell. This process can be mediated by various factors, including the lipid composition of the exosomes' membrane, integrins and the presence of fusogenic proteins (Gurung et al., 2021).

Endocytosis is the most common mechanism of exosomes uptake by recipient cells. This process involves the formation of a vesicle from the plasma membrane that encloses the exosomes and brings them into the cytoplasm. Endocytosis can occur through various pathways, including clathrin-mediated endocytosis, caveolin-mediated endocytosis, phagocytosis and macropinocytosis. Receptor-mediated uptake of exosomes uptake involves the binding of exosomes to specific receptors on the surface of the recipient cell. This mechanism allows exosomes to selectively target specific cell types or tissues (Amber, Ron, Janviere, Paul, & Nathan, 2019; Gonda, Kabagwira, Senthil, & Wall, 2019; Griffiths et al., 2022; McKelvey, Powell, Ashton, Morris, & McCracken, 2015; Mulcahy, Pink, & Carter, 2014).

1.5 The Mannose receptor

Dendritic Cells (DCs) play a critical role in the initiation and regulation of the immune response. DCs can be activated by various stimuli, including pathogens, danger signals, and cytokines, which can induce their maturation and enhance their ability to present antigens to T cells. An important role in the recognition of a variety of pathogen-associated molecular patterns (PAMPs), such as mannose, fucose, and N-acetylglucosamine present on the surface of pathogens, including bacteria, fungi, and viruses, is played by the Mannose Receptor (MR/CD206). MR is mainly

expressed on the surface of Antigen-Presenting Cells (APCs), such as dendritic cells (DCs), in particular immature DCs (iDCs), M2-type macrophages (M2 Φ), and some subsets of B cell. The mannose receptor is a member of the C-type lectin (CLEC) family, which can bind and internalize a variety of endogenous and pathogen-associated ligands by recognizing mannose, fucose, or GlcNAc residues in a calcium-dependent manner (Luisa Martinez-Pomares, Mantovani, & Stahl, 2023; Stahl & Ezekowitz, 1998; van der Zande, Nitsche, Schlautmann, Guigas, & Burgdorf, 2021).

The Mannose Receptor has 5 structural domains:

- an extracellular structural domain including an N-terminal cysteine rich region (CRD),
- a fibronectin type II domain (FN II)
- 8 C-type lectin-like domains (CTLD), a transmembrane region and a carboxy-terminal cysteine rich domain (Liu, Guan, Gao, Jiang, & Kang, 2017).

The MR constitutively recycles every 15 minutes between the plasma membrane and the early endosomal compartment, even in the absence of any ligand. Only 10–30% of the receptor is found at the cell surface and the remaining 70% is localised intracellularly (Gazi & Martinez-Pomares, 2009; Luisa Martinez-Pomares et al., 2023).

MR has been shown to play a role in antigen presentation. The MR-internalized antigens are directed toward early endosomes that do not mature and do not fuse with lysosomes. In this way antigens will not be degraded but will remain for longer times in the APCs and consequently will not be associated with the MHC II (Burgdorf, Kautz, Bohnert, Knolle, & Kurts, 2007; Burgdorf & Kurts, 2008; van der Zande et al., 2021). From this early endosomal compartment, MR-internalized antigens will be predominantly processed for antigen presentation on MHC I molecules by a process called cross-presentation (Burgdorf et al., 2007; Burgdorf, Lukacs-Kornek, & Kurts, 2006; Kreer, Rauen, Zehner, & Burgdorf, 2011).

1.6 Exosomes glycosylation

Since the mannose receptor plays an important role in antigen presentation, glycosylation of exosomes is an aspect that needs to be taken into consideration. Glycosylation is a post-translational modification consisting of the addition of one or more sugar units by an enzyme called glycosyltransferase and is an important process in the folding, maturation, trafficking and secretion, as well as in the function of proteins. The addition of a glycan precursor occurs initially in the endoplasmic reticulum and subsequently in the Golgi complex. Depending on the amino acid chain on which the sugars are linked it is possible to distinguish N-glycosylation (involving the side chain of an asparagine) and O-glycosylation (on a serine or threonine residue) (Kondo et al., 2022; Lin, Zhou, & Yuan, 2020). Recent studies conducted by using an array of lectins reported that exosomes contain high amounts of mannose and other classes of N-linked oligosaccharides (Krishnamoorthy, Bess, Preston, Nagashima, & Mahal, 2009; Shimoda, Sawada, Sasaki, & Akiyoshi, 2019; Surman et al., 2018; Williams et al., 2018).

A characteristic of the TME is the hypoxic condition. To survive and grow in this hypoxic microenvironment, tumor cells change their metabolism from oxidative phosphorylation to glycolysis, leading to modifications of glycosylation patterns, promoting proliferation. Cells become resistant to apoptosis obtaining unlimited replication potential, experience genomic instability, acquire the ability to evade immune attacks and to induce angiogenesis. Moreover glycosylation can promote metastasis generation (He et al., 2022; Martins, Ramos, Freitas, & Reis, 2021; Ruan, Song, & Ouyang, 2009; Surman et al., 2018). This condition of low oxygen may trigger variations in the molecular composition of exosomes released by primary tumor cells, including transmembrane and soluble proteins, mRNAs, and especially miRNAs which are involved in the suppression of M1 macrophage polarization (Banerjee et al., 2013; Ren et al., 2019; Ricklefs et al., 2019) and in the regulation of the inflammatory response in DC (Barutta et al., 2021; Saba, Sorensen, & Booth, 2014). Since exosomes reflect the lipid and protein profile of the cell of origin, it has been

observed that changes at the level of glycosylation are also acquired by these vesicles thus effectively making them potential biomarkers.

2. Aim of the work

All cells, both tumor and non-tumor, communicate with each other by releasing small Extracellular Vesicles (sEV) into the surrounding environment. In recent years, a crucial role has been attributed to exosomes, which are sEV formed through the inward budding of the membrane of Multivesicular Bodies (MVBs) that subsequently fuse with the plasma membrane releasing intraluminal vesicles into the extracellular space. Despite the extension of exosome studies to clinics, understanding important aspects of their biogenesis remains a longstanding goal, complicated by the heterogeneity among secreted vesicles with respect to their functionality (Kowal et al., 2016; Mathieu et al., 2021; Willms, Cabanas, Mager, Wood, & Vader, 2018; Zhang et al., 2018). Small vesicles that bud from the plasma membrane and share intrinsic characteristics with exosomes, such as molecular components or physical properties (size and floating density), have also been described, making their separation and characterization difficult (Jeppesen et al., 2019; van Niel et al., 2018; Zhang et al., 2018). To date, intracellular localization of exosome-specific molecules has mainly been determined by microscopy-based methods, but an actual understanding of late endosomes/MVB biogenesis requires the ability to more accurately establish the dynamics of organelle traffic leading to EV secretion. Different subpopulations of exosomes that coexist in the same MVB compartment can follow different intracellular pathways en route to release into the extracellular space, determining their molecular composition and ultimately the message delivered to target cells. Recently, new fluorescence labeling strategies ranging from novel lipid dyes to genetic labeling techniques have been developed to label EV or subtypes to track their biogenesis, biodistribution, and uptake (Lai et al., 2015; Mathieu et al., 2021; Verweij et al., 2021). However, the lack of suitable markers to specifically identify and separate EV subpopulations of different origins coexisting in secretory fluids complicates this process (Jeppesen et al., 2019; Nieuwland, Falcon-Perez, Thery, & Witwer, 2020; van Niel et al., 2022; Zhang et al., 2018), suggesting that tetraspanins alone cannot be used to distinguish between different types of EV (Karimi,

Dalirfardouei, Dias, Lotvall, & Lasser, 2022; Mathieu et al., 2021). To address this issue, new reliable experimental strategies are needed to identify specific exosome populations originating from late endosomes/MVBs. One of the less explored yet fundamental pathways of exosome biogenesis is the lipid pathway. With the aim of finding new strategies to obtain fluorescently labelled EV originating from an intracellular pathway, we previously exploited the lipid pathway using a fluorescent palmitic acid analog, BODIPY FL C16 (Bodipy C16). Bodipy C16 is readily internalized by cells and transformed into phospholipid components of sEV membranes, whose number and fluorescence intensity can then be precisely analyzed by flow cytometry (FC) (Coscia et al., 2016). In this study, we extended the characterization of fluorescent sEV (Bodipy sEV) to evaluate the general applicability of our method in obtaining a metabolically labeled subpopulation of sEV of intracellular origin, and excluding ectosomes contaminations. Thus, our approach represents a new and effective strategy for labeling a discrete exosome population that is distinct from ectosomes and can be further exploited for biogenesis and functional studies. Tumor cells release a greater quantity of exosomes compared to non-tumor cells that can transfer their oncogenic material altering the fate of recipient cells, thereby promoting tumor growth. The exosome-mediated transfer of molecular and genetic material between cells is a key contributor to intercellular communication involved in various physiological and pathological conditions. However, it is not known whether exosomes secreted by donor cells are selectively or non-selectively incorporated into recipient cells. Exosomes also play a role in modulating the Tumor Microenvironment (Ryan P. McNamara, 2021) in which tumor cells coexist with immune system cells. The main role in the TME is played by Antigen-Presenting Cells (APCs), immature dendritic cells (iDCs) and Tumor-Associated Macrophages (TAMs). iDCs have a key role in the immune response, they are the most potent professional APCs known, and it has been shown that iDCs internalize EVs more efficiently than mature dendritic cells, while the latter retain more EVs on the cell surface (Montecalvo et al., 2008). iDCs express high levels of

mannose receptor (MR/CD206), a lectin like receptor of the innate immune system (Anneke J. Engering, Fluitsma, & Elisabeth C. M. Hoefsmit, 1997; Ezekowitzt, 1998; Taylor, Gordon, & Martinez-Pomares, 2005). Exosomes are extremely enriched in high-mannose residues and recent studies show that cellular and exosomal glycosylation profiles are modified in hypoxic conditions such as those found in the TME (Echevarria et al., 2014; Kondo et al., 2022; Williams et al., 2019). In the second part of this project, our aim was to investigate whether exosomes, derived from melanoma A375/M cells cultured under normoxic (21% O_2) or hypoxic (5% O_2) conditions, could be selectively internalized via the Mannose Receptor (MR/CD206) expressed on iDCs. Additionally, we aimed to observe if exosomes could induce cells differentiation into the mature phenotype.

3. Results

3.1 Bodipy C16 internalization and sEV secretion in human cell lines

We previously showed (Coscia et al., 2016) that Bodipy C16, a fluorescent analog of palmitic acid, is rapidly internalized by cells and metabolized into phospholipids that enter the EV biogenesis pathway, ultimately producing fluorescent sEV. To extend our observations we first evaluated the intracellular distribution of Bodipy C16 in a panel of five human cell lines, three melanoma (Mel501, Me665/1 and A375/M) and two cell lines frequently used in sEV studies (HEK293 and HeLa). Confocal images of all the tested cell lines showed intense fluorescence distributed in the perinuclear region and in discrete structures compatible with endolysosomal compartments after 2 h of Bodipy C16 uptake (Figure 1a), whereas the fluorescence signal appeared absent from the plasma membrane. No noticeable differences were observed among the different cell lines. We next compared the secretion of Bodipy sEV over a 24 h period to highlight any potential differences in secretion among the cell lines. Due to varying cell duplication rate, we evaluated the number of secreted Bodipy sEV per single cell, based on the effective number of cells recovered at the end of the 24 h period (Figure 1b). Cells exhibited different levels of sEV secretion with the highest amount generated by the Mel501 cell line that was chosen for further studies. Palmitic acid has been shown to be toxic to mammalian cells in a concentration-dependent and time-dependent manner, inducing cellular dysfunction, ER stress, and cell death (Akoumi, Haffar, Mousterji, Kiss, & Bousette, 2017; Malhi, Bronk, Werneburg, & Gores, 2006; Penke et al., 2017). In addition, it has been reported that palmitic acid treatment increases exosome production in hepatoma cell lines, although this effect was observed at an almost millimolar concentration range (Y. S. Lee et al., 2017). To rule out a potential effect of Bodipy C16 on sEV secretion, we treated Mel501 cells with 7 μM Bodipy C16 or equivalent concentrations of unlabeled palmitic acid for 5 h in cell labeling medium. Then, we chased the cells for 24 h in EV-depleted complete medium. The results indicated that

there were no significant effects of palmitic acid or Bodipy C16 on the total amount of sEV secretion detected by NTA (Figure 1c) or on the levels of well-known sEV markers such as CD63, CD81, CD9 and TSG101 (Figure 1d), compared to the untreated control cells. Therefore, we were able to rule out any effect of palmitic acid at the concentrations used on sEV secretion.

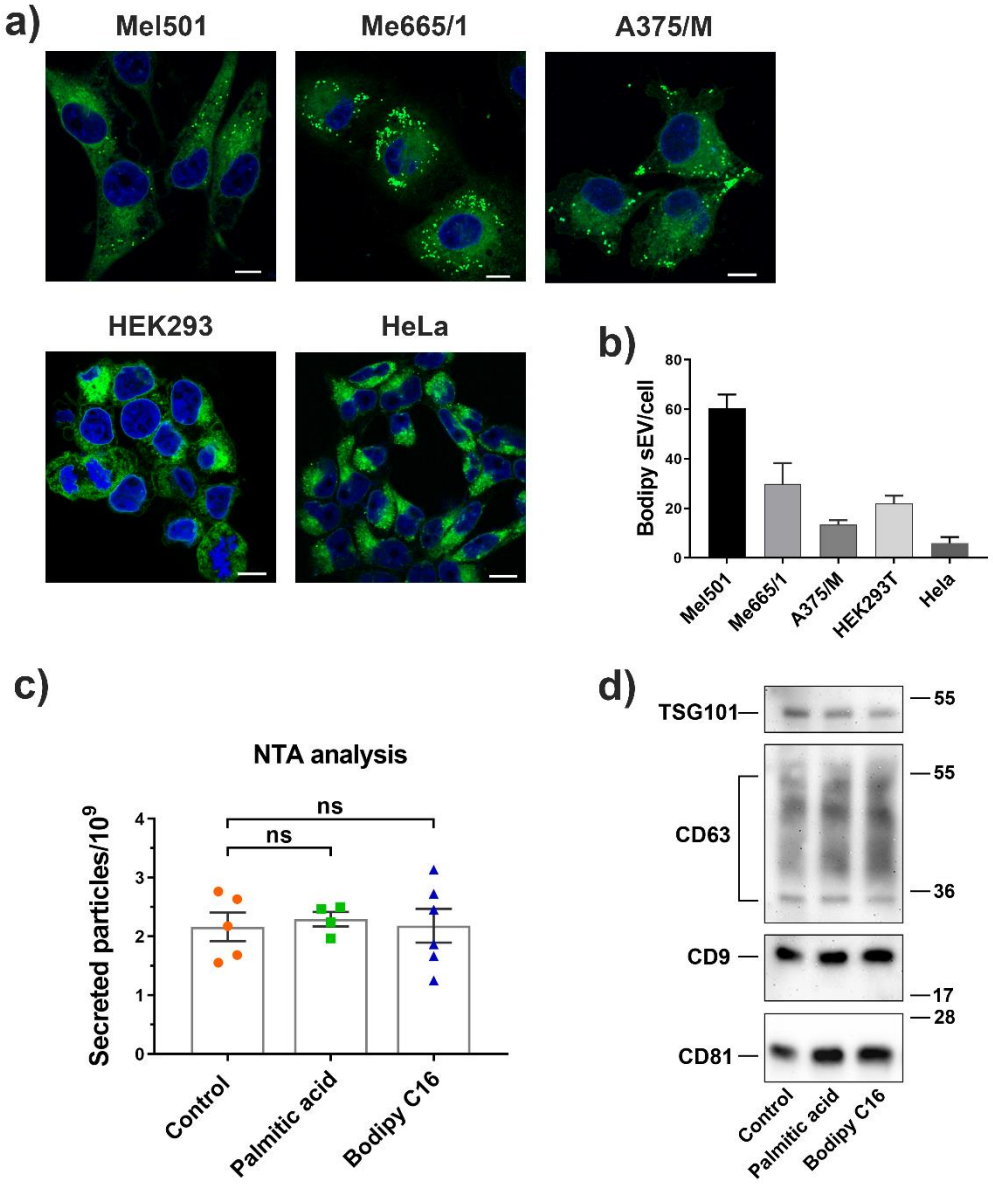

Figure 1. (a) Confocal microscopy images of cells labeled for 2 h with Bodipy C16 at steady state. **(b)** Quantification by Flow Cytometry (FC) of sEV secreted in the conditioned medium of different cell lines. **(c)** Measurement by Nanoparticle Tracking Analysis (NTA) of total sEV released by Mel501 cells untreated or treated with Bodipy C16 or with unlabeled palmitic acid for 5 h. SEV were purified from

conditioned media after 24 h of chase. Bars represent the mean ± SEM (n > 3). **(d)** Western blot analysis of total sEV released by untreated or treated with Bodipy C16 or with unlabeled palmitic acid.

3.2 Bodipy C16 is transformed into phospholipids in melanoma cell

Palmitic acid plays a central role in the synthesis and maintenance of structural phospholipids and in cancer cells exogenous palmitate has been found to be incorporated into various lipids required for their proliferation and pro-tumorigenic lipid signaling (Louie, Roberts, Mulvihill, Luo, & Nomura, 2013). In addition, various in vitro and in vivo studies have shown that palmitic acid overload causes increased triglyceride accumulation into lipid droplets (LD) (Olzmann & Carvalho, 2019) and it is often used in vitro to induce lipid droplet formation (Thomas et al., 2022). To gain better insight into the metabolic transformation of Bodipy C16 within the cells, we first performed a time course experiment of Bodipy C16 uptake. We have previously reported that the optimal concentration of Bodipy C16 for probe incorporation is 7 μM (Coscia et al., 2016) which is much lower than that reported for the induction of lipid droplet formation or cytotoxic effects (Thomas et al., 2022). To further characterize the time course of Bodipy C16 uptake and metabolism we pulsed cells with the probe for different times and measured cell associated fluorescence by FC. Bodipy C16 uptake reached saturation at 5 h (Figure 2a). When the cells were incubated with the probe for 5 h and then washed and chased in fresh medium, a sharp decrease of total cell fluorescence was observed after 1 h, with 50% of the initial fluorescence reached at 6 h (Figure 2b). Subsequently, fluorescence levels decreased more slowly (Figure 2b). Next, we performed lipid extractions of cells that had been pulsed with Bodipy C16 for 15 min, washed and then chased in fresh media for up to 24 h and analyzed. As illustrated in Figure 2c, cells pulsed with Bodipy C16 for a short time, very rapidly metabolized the Bodipy C16 into phospholipids and neutral lipid intermediates, visible already at the end of the pulse time. These latter rapidly decreased over time and were significantly reduced by about 30 min of chase thus demonstrating that the observed intracellular fluorescence did not result from free probe diffusing in the cells either alone or bound to the BSA used as carrier. To

identify all possible fluorescent lipid intermediates, we increased the pulse time to 5 h and collected cells and sEV after 2 h and 24 h of chase (Figure 2d). In these conditions, we observed the appearance of fluorescent phospholipids and neutral lipid intermediates but not of triacylglycerols (TAG), diacylglycerols (DAG), or cholesterol in cell extracts. This finding suggests that at the low concentrations used, Bodipy C16 is not transformed into TAG and cholesteryl esters, which are the main constituents of the neutral lipid core of lipid droplets (Pol, Gross, & Parton, 2014). Notably, fluorescent lipids in sEV were mainly associated with phospholipids. Total lipids from both cells and sEV were then extracted and resolved for phospholipids (Figure 2e). In the cell extracts, phospholipids content greatly decreases with time, while the sEV extracts did not exhibit changes in phospholipids associated fluorescence intensity, even after 24 h. Our results show that in melanoma cells Bodipy C16 is a precursor of the de novo biosynthesis of phospholipids that enter membranes biosynthesis pathway.

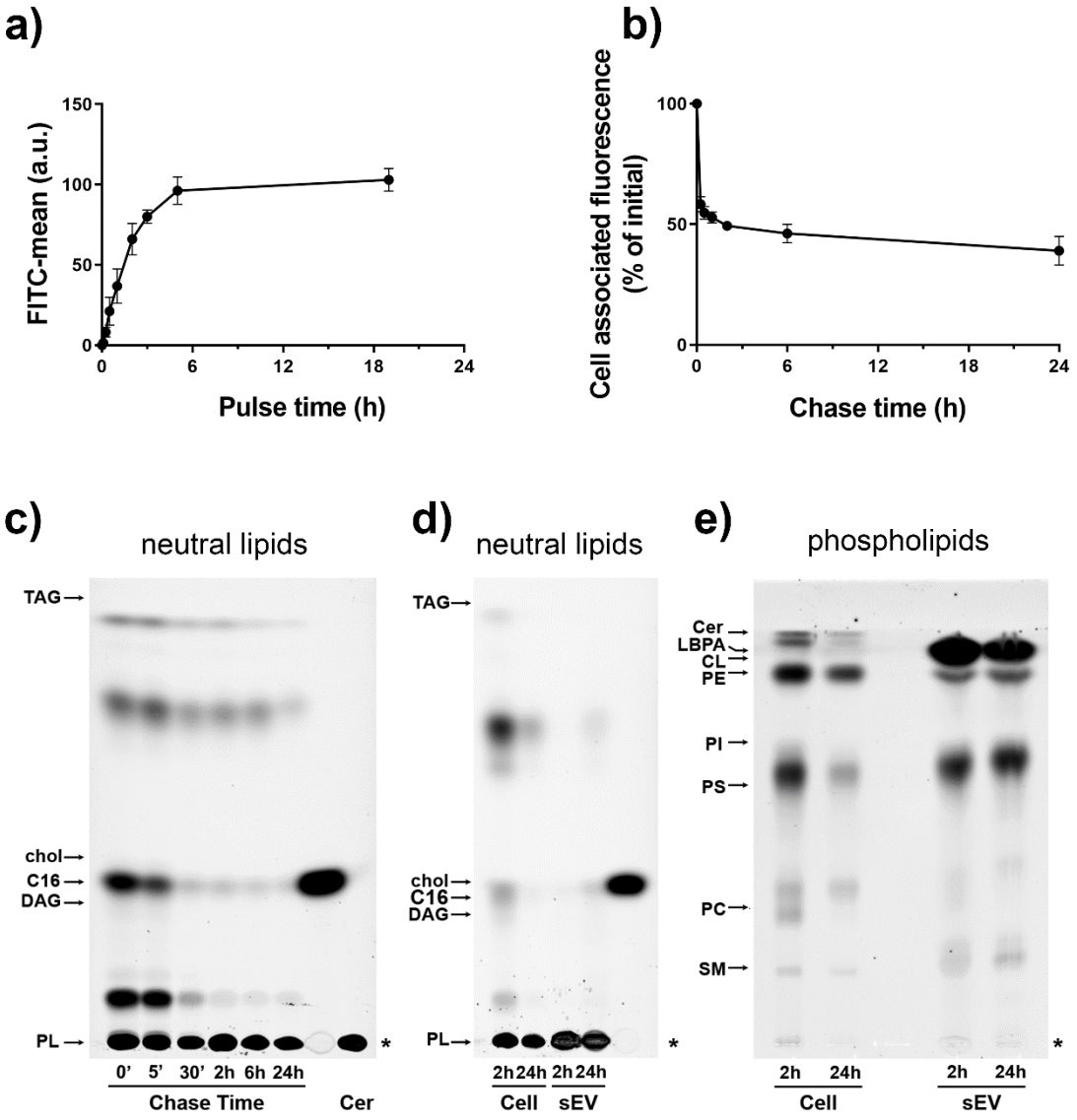

Figure 2. Dynamics of Bodipy C16 uptake and transformation into phospholipids. (a) Mel501 cells were treated with 7 μM Bodipy C16 for the indicated times or **(b)** treated for 15 min, washed with H-BSA and chased in complete medium. Cell associated fluorescence was measured by FC. Data are expressed as mean ± SEM (n = 3). **(c)** Total lipids from cells pulsed with Bodipy C16 for 15 min and chased for different times were extracted and analyzed by HPTLC. The amount of lipid spotted per lane was equivalent to $5x10^4$ cells. **(d)** Lipids from $2x10^4$ cells pulsed with Bodipy C16 for 5 h and chased for 2 h and 24 h and Bodipy sEV isolated from the conditioned medium were extracted and analyzed by HPTLC for neutral lipids and **(e)** phospholipids. The amount of lipid spotted per lane was equivalent to $4x10^4$ cells and $8{,}6x10^8$ sEV. Asterisk indicates the sample origin line. Lipids were identified based on comparison to the respective lipid standards. Neutral lipids: TAG, triacylglycerols; DAG, diacylglycerol; chol, cholesterol; C16, Bodipy C16; PL, Polar Lipids. Phospholipids: Cer, ceramide; LBPA, Lysobisphosphatidic acid; CL, cardiolipin; PE, phosphatidylethanolamine; PI, phosphatidylinositol; PS, phosphatidylserine; PC phosphatidylcholine; SM, sphingomyelin.

3.3 Bodipy C16 labels membranes of the ER/endolysosomal compartment

To investigate the intracellular journey of Bodipy C16, which leads to fluorescent sEV release, we initially examined whether Bodipy C16 is transported to mitochondria and lysosomes, organelles involved in fatty acid metabolism. We pulsed cells with Bodipy C16 for short periods (15 min and 30 min) and tracked its colocalization with the mitochondrial marker MitoTracker and LysoTracker, a cell permeable weak base dye that accumulates in acidified organelles. As shown in Figure 3a and Figure 3b, the Bodipy green fluorescent signal colocalized with MitoTracker (red) by about 40% and with LysoTracker (red) by about 30% after 15 min of Bodipy C16 uptake. At 30 min, we observed persistent colocalization of the fluorescent signal with mitochondria, while colocalization with lysosomes showed a significant decrease to about 41% of the initial value. These experiments suggest that upon uptake, Bodipy C16 is quickly targeted to organelles where lipid transformation may commence. To assess the degree of colocalization between Bodipy FL C16 and endogenous marker proteins targeting different locations on the endocytic pathway, we conducted confocal immunofluorescence experiments. As a first step, we aimed to establish whether lipids derived from Bodipy C16 colocalized with the plasma membrane, in order to exclude the possibility of fluorescent sEV originating from it. For this purpose, we pulsed cells with Bodipy C16 for 2 h (Figure 3c) and examined the colocalization with the lectin Concanavalin A (Con A), which labels the plasma membrane. The analysis of colocalization, as shown in Figure 3d, indicated that there was almost no colocalization, as only 0.8±0.1% SEM of Bodipy fluorescence was found at the plasma membrane. We then established the colocalization with Con A as a baseline for comparison with other markers. Next, we utilized Phalloidin, which stains polymerized actin, to outline the cell periphery. The colocalization with this marker was poor (3.7±0.4%), further suggesting that Bodipy C16 derived phospholipids are not trafficked to the plasma membrane but follow different intracellular routes. Since the trans-Golgi network and endoplasmic reticulum (ER),

in addition to being main sites of membrane lipid synthesis (Fagone and Jackowski, 2009), are organelles known to contribute to the formation of the early-sorting endosome that eventually generates MVB (Kalluri and LeBleu, 2020), we analyzed colocalization with ER and Golgi markers. As expected, we found significant colocalization with calregulin (14.4±2.3%) and calnexin (19.7±2.7%), and GM130 (24.1±3.3%) (Figure 3d), indicating that 2 h after the addition of Bodipy C16, fluorescent lipids are present in these compartments presumably en route to compartments from which intraluminal vesicles are generated. Finally, we determined colocalization with the protein markers CD63, CD81, and CD9, which are commonly used to identify sEV, and with LBPA, an atypical lipid highly enriched in late endosomes/MVB (Kobayashi et al., 1998; Gruenberg, 2020). As shown in Figure 3c and 3d we found high colocalization with CD63 (17.8±1.8%), and CD9 (14.4±1.5%) and lower but significant colocalization with LBPA (9.1±0.7%). It has to be noted CD9 staining exhibited a punctate distribution pattern within intracellular compartments, which differs from the predominantly plasma membrane localization observed in HeLa cells (Mathieu et al., 2021). Conversely, colocalization with CD81 was low (2.4±0.3%) consistent with previous observations that CD81 is mostly localized to the plasma membrane (Fordjour, Guo, Ai, Daaboul, & Gould, 2022; Larios, Mercier, Roux, & Gruenberg, 2020) and further supporting the hypothesis that Bodipy lipids are not targeted to the plasma membrane. Taken together these results provide evidence that upon internalization Bodipy C16 rapidly localizes in lipid metabolism sites where transformation in phospholipids likely occurs, and that the lipids derived from Bodipy C16 become a part of the late endosome membranes with the exclusion of the plasma membrane.

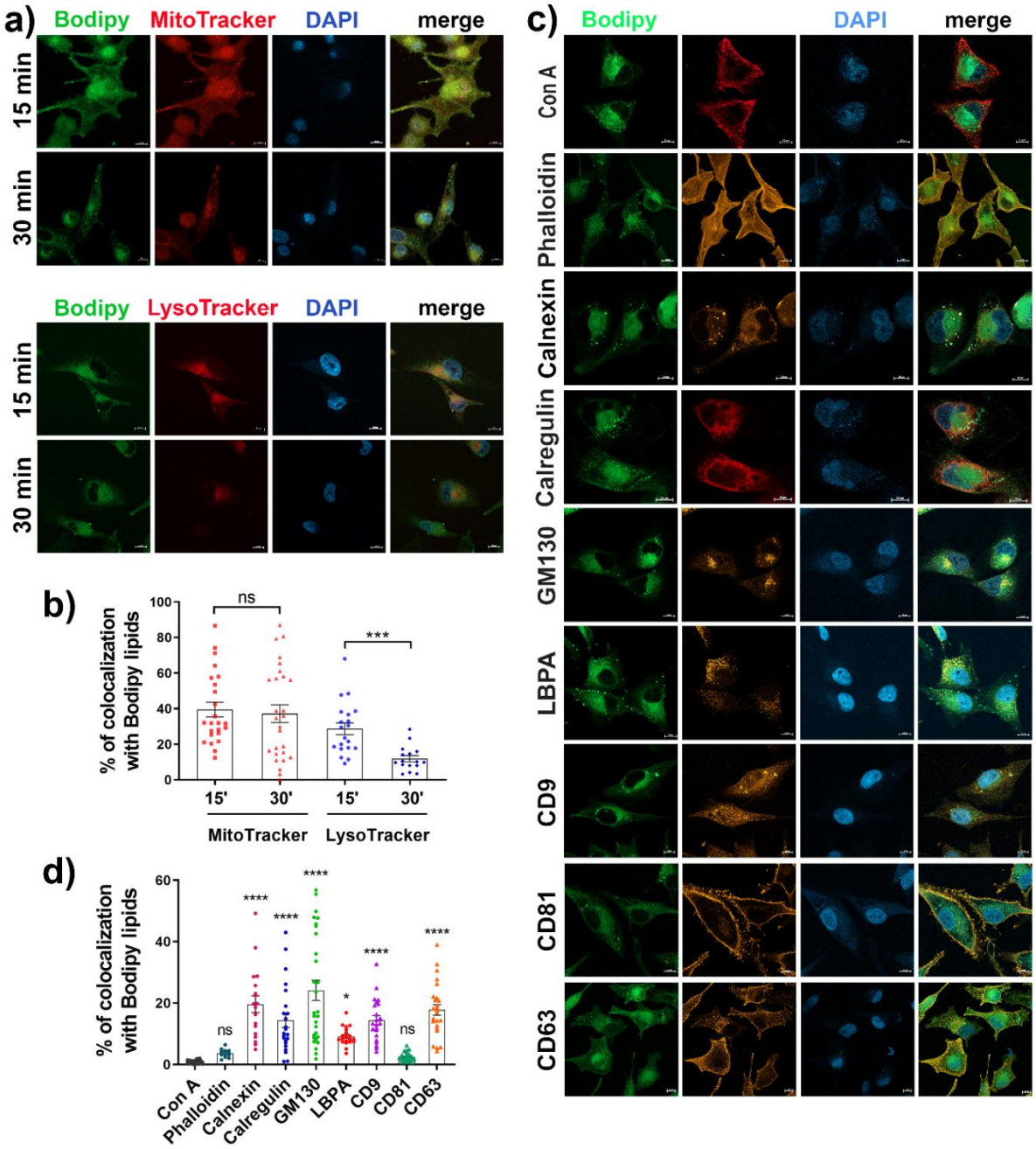

Figure 3. Co-localization analysis of Bodipy lipids with intracellular markers. **(a)** Colocalization with mitochondria and lysosomes at different pulse time. Cells were labeled with 1 µM Bodipy C16 and Mitotracker Deep Red or Lysotracker Deep Red for 15 or 30 min, fixed and mounted with DAPI. **(b)** Quantification of colocalization with Bodipy lipids. Quantification of 3 independent experiments showing the mean ± SEM (≥20 fields). **(c)** Colocalization of Bodipy lipids with intracellular organelles markers and tetraspanins after a 2 h pulse with Bodipy C16 at steady-state. Fixed cells were permeabilized with 0,1% saponin prior to incubation with antibodies or non permeabilized when incubated with Con A. Percentage of colocalization is calculated by summing the pixels in the colocalized region and then dividing by the sum of Bodipy C16 pixels. All data are expressed as means ± SEM (n ≥ 3) (n ≥ 20 fields). Individual unpaired t-test was performed to compare two groups. Significance of colocalization in **(d)** was calculated by comparing percent of individual markers colocalization with Con A colocalization. *p < 0.05, **p < 0.01, ***p< 0.001, ****p< 0.0001, ns, no statistical significance. Scale bar=10 µm.

3.4 Bodipy sEV are a homogeneous subpopulation of EV

Previous reports have shown that cells release subpopulations of exosomes differing in molecular and biophysical properties such as density range of sedimentation, and that these can be separated by density gradient centrifugation (Kowal et al., 2016; Willms et al., 2016; Zhang et al., 2018). To address the question of whether Bodipy sEV represent a specific subpopulation of sEV we subjected the conditioned media of Mel501 cells pulsed with Bodipy C16 and chased for 24 h, to differential centrifugations to obtain an ultracentrifugation pellet (100,000g = 100K), classically considered as containing exosomes. The resulting pellet was loaded at the bottom of an iodixanol gradient, followed by ultracentrifugation for 16 h to allow vesicles to float into the gradient. The distribution of fluorescent sEV within the gradient fractions was analyzed by FC. Bodipy sEV were separated as a discrete peak in fractions 4-5 (density range 1.067-1.081 g/ml, as measured by refractometry) (Figure 4a, 4c). These fractions contained the exosome marker proteins CD63, CD81, CD9, Alix, and Syntenin 1, as well as Annexin 1, a marker of microvesicles shed from the plasma membrane (Jeppesen et al., 2019), which showed a similar distribution (Figure 4d). To be noted, the density range of the Bodipy sEV was lower than that previously reported for exosomes (Colombo et al., 2014; Willms et al., 2016). To rule out the possibility that Bodipy sEV were an artifact, we added to the gradient fractions low concentrations of octyl-glucoside (OG) (60mM), a nonionic detergent widely used for membrane protein solubilization, in order to discriminate between protein aggregates and membrane vesicles (Inglis et al., 2015; Jeppesen et al., 2019). As shown in Figure 4a, OG completely abolished fluorescent particles detection in the low-density fractions, thus confirming that Bodipy sEV are indeed membrane-enclosed vesicles. Since floatation of sEV bottom loaded into Iodixanol gradients has been widely used to separate distinct subpopulations of sEV, we incubated 100K pellets containing the total population of sEV derived from conditioned media of untreated Mel501 cells, with CFSE, a cell permeable protein-binding dye commonly used to obtain fluorescently labelled sEV preparations (Groot Kormelink et al., 2016;

Morales-Kastresana et al., 2017; Pospichalova et al., 2015; Woud et al., 2022). The total CFSE sEV pellets were subjected to iodixanol density gradient centrifugation and the fractions analyzed by FC. As shown in Figure 4b, CFSE vesicles separated into two distinct peaks, a lower density peak in the same density range as Bodipy sEV and a higher density peak that was only partially soluble with detergent, consisting mostly of protein aggregates. This suggests that the higher density peak contains a small proportion of membrane vesicles along with non-vesicular contaminants that co-isolated with the sEV during the purification process.

In recent years, several reports have shown that sEV of endosomal origin are enriched on their surface in CD63, CD81 and CD9 tetraspanins although in different combinations and amounts and depending on the cell type (Hurwitz, Conlon, Rider, Brownstein, & Meckes, 2016; Kowal et al., 2016; Willms et al., 2016). To characterize the Bodipy sEV population comprised in the 100K pellet among microvesicles and other particles we performed colocalization experiments of Bodipy sEV with fluorescent-labelled antibodies against CD9, CD63 and CD81 (Ricklefs et al., 2019). Results show that 14.2% of Bodipy sEV were $CD63^+$, whereas $CD81^+$ and $CD9^+$ amounted respectively to 8.1 % and 3.1%. Double positive $CD63^+/CD81^+$ were 3.9%, $CD81^+/CD9^+$ were 1.2% while $CD63^+/CD9^+$ were only 0.6 % of the total positive vesicles, supporting the hypothesis that Bodipy sEV represent a distinct low density subpopulation of sEV of endosomal/MVB origin (Figure 4e).

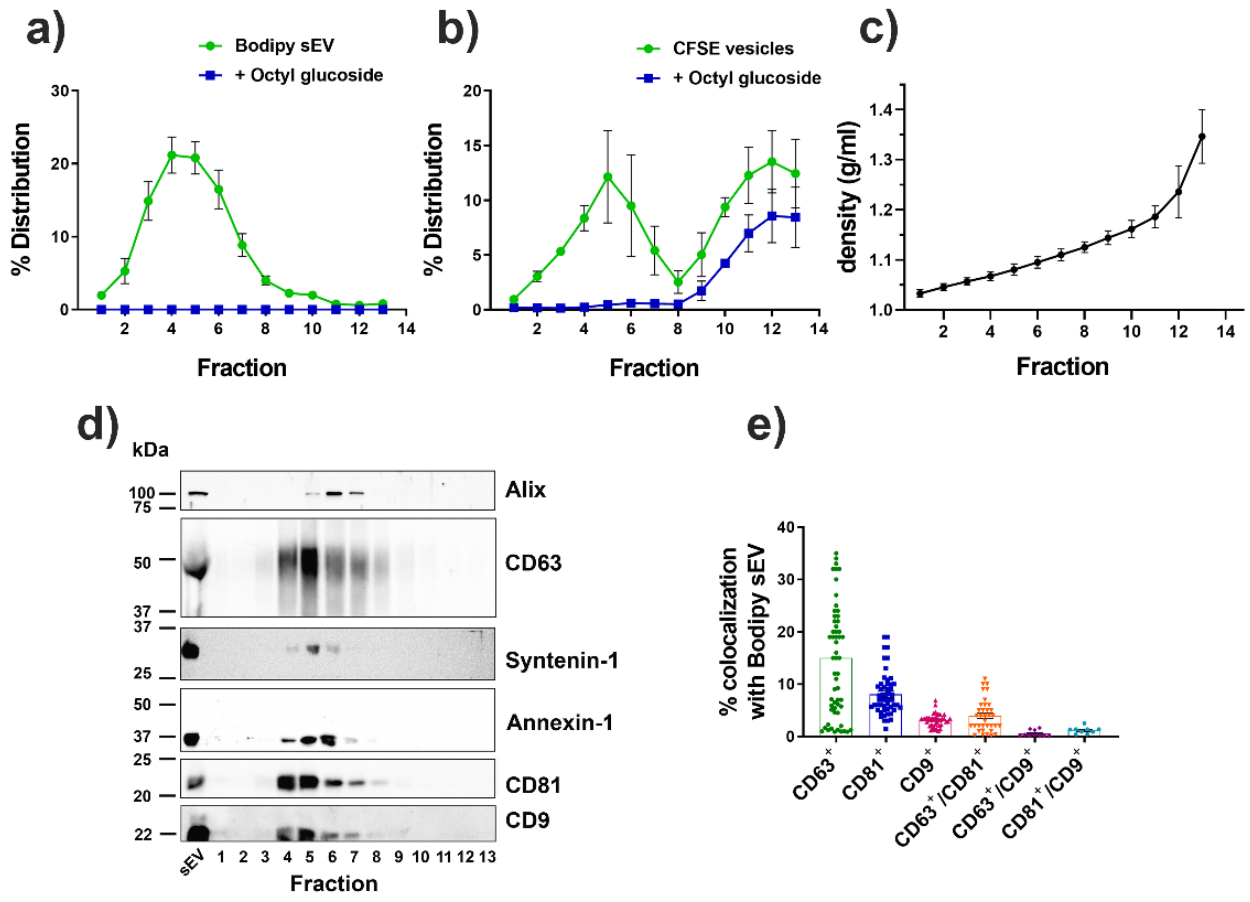

Figure 4. Bodipy sEV separate as a single peak enriched in tetraspanins. **(a)** Bodipy sEV 100K pellets were loaded at the bottom of an iodixanol density gradient and ultracentrifuged for 16 h. Fractions were collected from the top of the gradient and were analyzed for Bodipy sEV number by FC before and after the addition of 60 mM Octyl-beta-glucoside (OG). Data are expressed as mean ± SEM (n=14). **(b)** 100K pellets from conditioned media of untreated Mel501 cells were incubated with CFSE to non specifically label the total population of sEV and loaded at the bottom of an iodixanol density gradient. Data are expressed as mean ± SEM (n=4). **(c)** Density of the fractions was measured by refractometry. Data are expressed as mean ± SEM (n=17). **(d)** The total volume of each fraction was analyzed by Western blot. Data shown are representative of three independent experiments. **(e)** Analysis of colocalization of tetraspanins fluorescent antibodies with Bodipy sEV.

3.5 Kinetic of Secretion of sEV

The regulation and kinetics of exosome secretion have not yet been well characterized due to the lack of suitable methods to distinguish between subpopulations of sEV. However, our methodology allows for the analysis of a distinct population of vesicles of intracellular origin. Therefore, to trail the dynamics of Bodipy sEV release we set up experiments to determine the kinetics of Bodipy sEV secretion in Mel501 cells and determine if there is a correlation between cell fluorescence decrease (Figure 1b) and fluorescent sEV secretion. We pulsed cells with Bodipy C16 for 2 h, washed the cells, and chased them in fresh medium. Conditioned medium was harvested at different time points to determine the number of Bodipy sEV secreted. The results show that at 6 h of chase, the number of Bodipy sEV released in the conditioned media reaches a plateau, and there is no further increase at 24 h (Figure 5a). As control, we determined the kinetics of Bodipy sEV release in conditioned media in comparison with the total particles present in the same 100K pellet. NTA quantification of the total particles in the same sample showed a similar kinetics up to 6 h, steeply increasing at later time points (Figure 5b). This is supported by the ratio of Bodipy sEV secretion versus total particles, which is constant up to 6 h with approximately 4.5 times more particles than Bodipy sEV (Figure 5c). However, at 24 h, this ratio is 11, indicating that the intracellular Bodipy C16 reservoir is depleted in the first few hours after the Bodipy C16 pulse, as Bodipy phospholipids are trafficked to sites where ILV are formed and readily secreted. Once Bodipy labeled sEV are released, the secretion of unlabeled sEV takes over. Western blot analysis of 100k pellets collected at different time points show the increase over time of CD63, CD81, and CD9 tetraspanins (Figure 5d) reflecting the kinetics of Bodipy sEV secretion. CD63, which is highly enriched on ILVs in late endosomal MVB, is detected first at 30 min followed by CD81, whereas CD9 a marker that in recent studies is more often associated with ectosomes (Mathieu et al., 2021) becomes detectable at later time points. In conclusion, the data presented collectively indicate that the metabolic labeling methodology described in this study provides

the means to distinguish between various subpopulations of sEV and accurately monitor the release dynamics of Bodipy-labeled sEV.

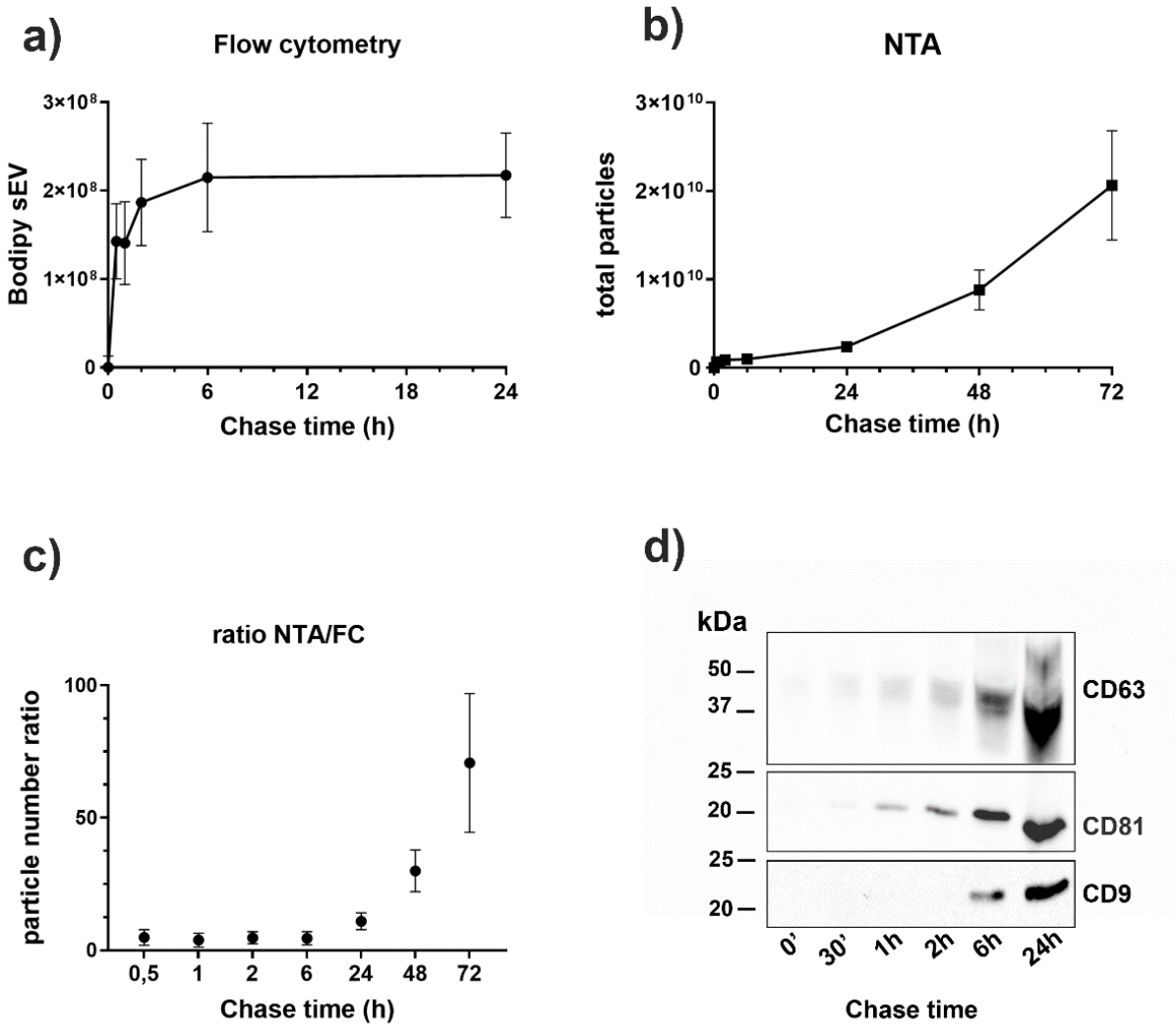

Figure 5. Secretion kinetics of Bodipy sEV. Cells were pulsed with Bodipy C16 for 2 h and chased for different times. The number of purified sEV purified by differential ultracentrifugation was measured by **(a)** FC or by **(b)** Nanoparticle Tracking Analysis (NTA). Results are expressed as means ± SEM of at least 6 independent experiments. **(c)** Ratio between the total number of sEV counted by NTA and Bodipy sEV counted by FC. A constant ratio is showed up to 6 h, while there is an increase of total vesicles over the time. Results are expressed as means ± SEM of at least six independent experiments. **(d)** Representative Western blot analysis of tetraspanins expression in Bodipy sEV secreted at different chase time. The total sEV released at each time point has been analyzed.

3.6 Bodipy sEV are a subpopulation of small exosomes

Recently, it has been shown that high-sensitivity flow cytometers can discriminate sEV in the range of 100 nm that can be efficiently sorted (Morales-Kastresana et al., 2019). Analysis and sorting of both sEV and larger EVs with multiplex fluorescent detection requires fluorescent labeling of the vesicles that can be obtained in multiple ways such as generic labelling of the EV surface (Morales-Kastresana et al., 2019), incorporation of fluorescence protein tags (i.e. GFP or fluorescent immunostaining using antibodies to specific surface biomarkers on EV. However, all these methodologies still need to be implemented since no generic marker can stain all sEV or more specifically a specific subpopulation of sEV like exosomes. We took advantage of our metabolically labelled Bodipy sEV to investigate the possibility of obtaining a pure population of Bodipy-labeled sEV by sorting the Bodipy-positive population using a MoFlo Astrios-EQ instrument.

To assess the background noise, we used PBS, while unlabelled sEV were used to evaluate the non-fluorescent signal (Figure 6a, left dot plot). The representative sorting in Figure 6a shows the total EVs, with the middle dot plot indicating that the Bodipy+ sEV account for 50% of the total EVs. After sorting, the percentage of purified Bodipy+ sEVs increases to 66% (Figure 6a, right dot plot). It is important to note that the background noise cannot be completely eliminated as it is intrinsic to the system, as previously described (Morales-Kastresana et al., 2017). Nonetheless, the sorting procedure allowed for the isolation of the Bodipy-positive sEV population, that can be used for further analysis.

Bodipy-labeled sEV were validated using transmission (TEM) and scanning (Ricklefs et al., 2019) electron microscopy. Fresh preparations of total unlabeled sEV or total Bodipy-labeled sEV were examined by TEM to assess their morphology and integrity (Figure 6b)01 Moreover, SEM micrographs of total Bodipy-labeled sEV show a heterogeneous mixture of vesicles with a median size of the major diameter of 98 nm (Figure 6d). NTA analysis of the same samples gave an even higher mode size of 120 nm, consistent with the fact that NTA cannot distinguish between effective vesicles

and other types of aggregates that are present in the vesicle preparations. SEM analysis of total Bodipy-labeled sEV analyzed before (Figure 6c, left) and after sorting (Figure 6c, right) exclusively reveal that sorted Bodipy positive sEV are a more homogeneous population of vesicles emerging in a very low background (Figure 6c, right). The semi-quantitative EM analysis of the size distribution of these population of vesicles (n >100) shows a median value of 80 nm, significantly smaller than that of the total EV ($p<0,001$) (Figure 6d).

The immunogold labelling of total EVs with anti-Bodipy FL antibodies shows low levels of the gold signal in the Bodipy+ sEV (Figure 6e, middle right) suggesting that the Bodipy epitope is not as readily exposed as the tetraspanin antigens, indicating potential differences in the accessibility of the antigens on the sEV membrane. In contrast, the anti-CD81 antibodies as well as anti-CD63, easily recognize the respective antigens around the exosome surface (Figure 6e, left and middle left). The image presented in Figure 6e (Hoshino et al.) provides evidence of colocalization between CD63 (10 nm) and Bodipy (5nm) antigens on the same vesicle, confirming that the Bodipy sEV analyzed by immune-electron microscopy indeed exhibit Bodipy positivity in accordance with the relative percentage observed in flow cytometry data. Taken together these results indicate that the Bodipy labelled sEV are a discrete subpopulations of small exosomes valuable for further characterization and exosome biogenesis studies.

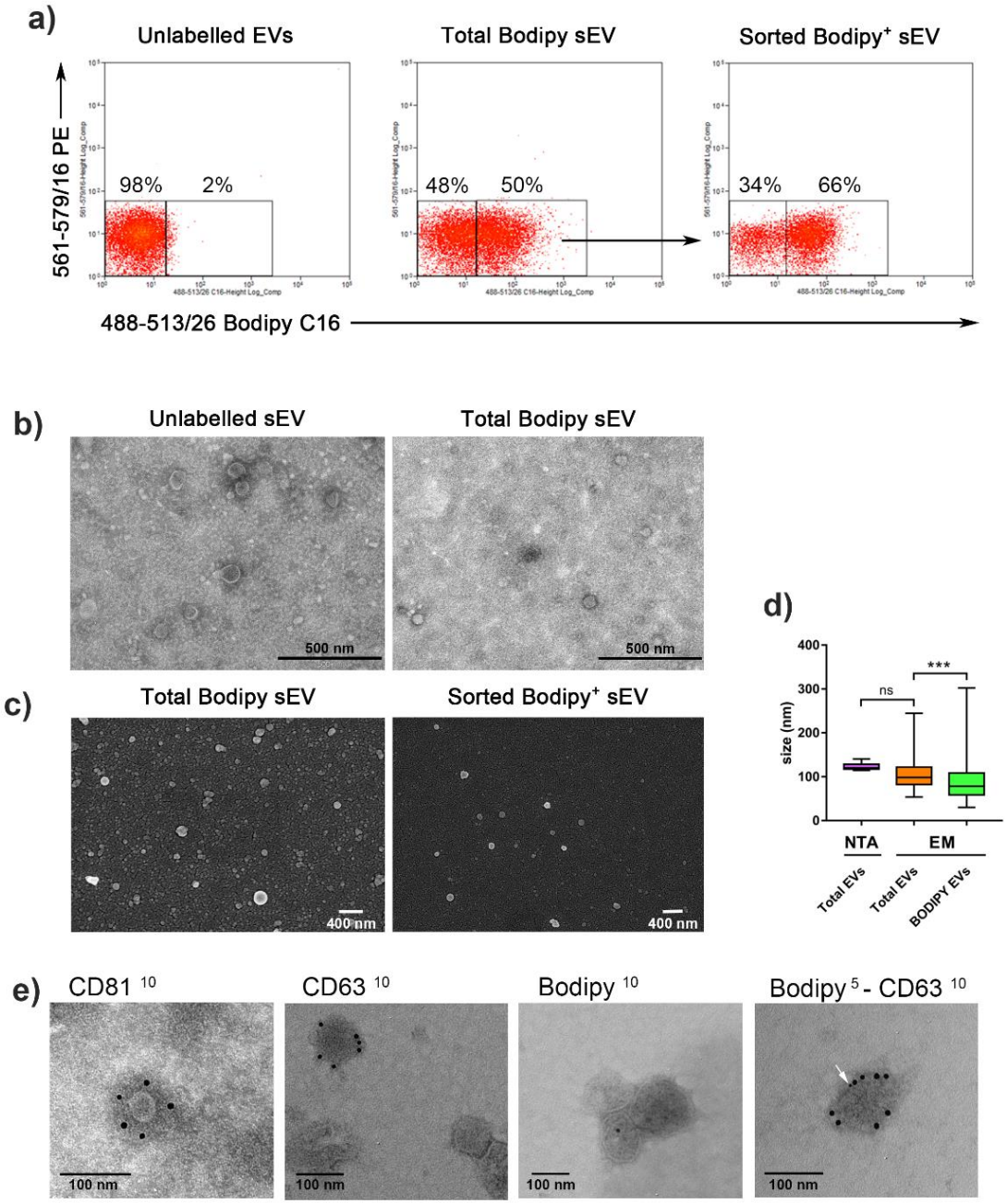

Figure 6. **Bodipy sEV can be sorted in a homogenous subpopulation of small exosomes**. **(a)** Fluorescent sEV pellets have been sorted with a MoFlow AstriosCell Sorter. Dot plot on the left shows unlabeled EVs. The dot plot in the middle shows total Bodipy+ sEV and the arrow indicates the region used for sort decision. The post sorting analysis shows purified Bodipy+ sEV (dot plot on the right). Dot plots are representative of three independent experiments. **(b)** Unlabeled sEV and total Bodipy+ sEV were analyzed by TEM showing the presence of a discrete population of membrane vesicles in both samples. **(c)** FACS sorted Bodipy+ sEV analyzed by SEM revealed a homogeneous population of small vesicles in a very low background (Hoshino et al.), particularly appreciable when compared directly to the total Bodipy-labeled sEV population. (left). **(d)** Total sEV size was determined by NTA and electron microscopy (EM) The semi-quantitative EM analysis (N>100) showed that the sorted Bodipy+ sEV had a median size of 80 nm, significantly smaller than total Bodipy-labeled sEV population (*** p<0,001). **(e)** Total sEV were immunolabeled

with anti CD81, CD63 and Bodipy antibodies, revealed by 10 nm colloidal gold conjugated secondary antibodies (left, middle left and middle right TEM micrographs). Colocalization of CD63 (10nm) and Bodipy (5nm, white arrow) antigens on the same vesicle is shown in the right image.

3.7 Characterization of Bodipy exo under normoxic or hypoxic conditions

Tumors secrete higher levels of exosomes than non-tumoral cells, which can transfer oncogenic cargo, including proteins, nucleic acids, and miRNAs to recipient cells and alter their behaviour thus promoting cancer cell survival and growth. Hypoxia is a typical feature of the tumor microenvironment and this condition of low oxygen may trigger variations in the molecular composition of exosomes released by primary tumor cells. Exosomes possess high amounts of mannose and other classes of N-linked oligosaccharides on their surface, which are altered in the hypoxic condition found in the TME (Gerlach & Griffin, 2016; Shimoda et al., 2019; Surman et al., 2018; Williams et al., 2018). Due to these alterations, we opted to employ the Bodipy C16 labelling method to examine any differences between exosomes obtained by melanoma cells A375/M cultured under normoxic (21% O_2) or hypoxic (5% O_2) conditions pulsed with Bodipy (Bodipy exo). Bodipy exo have been quantified by flow cytometry (FC) and characterized for the expression of typical exosomal markers, in particular tetraspanins CD63, CD81, CD9 and for their mannosilation profile. Bodipy exo have been incubated with antibodies anti-CD63 BV421, anti-CD81 APC and anti-CD9 PE and the percentage of colocalization with C16 was evaluated by FC. To analyze the glycosylation profile, the mannose-binding lectin Concavanalin A (Con A) conjugated with Alexa Fluor 647 has been used. Con A is a lectin that specifically binds α-D-mannosyl and α-D-glucosyl residues, interacting with different receptors containing mannose carbohydrates and also with mannose residues on the surface of many bacteria. The analysis showed that Bodipy exo secreted under both conditions presented a similar percentage of colocalization with the three tetraspanins while hypoxic exosomes showed a percentage of colocalization

with Con A almost 40% that is significantly higher than normoxic exosomes which is about 30% (Figure 7a). To confirm the binding of Con A with the mannose residues on Bodipy exo, yeast mannan was used as binding competitor. The analysis showed that in presence of y.mannan there was a significant decrease of the percentage of colocalization between Con A and Bodipy exo (Figure 7b).

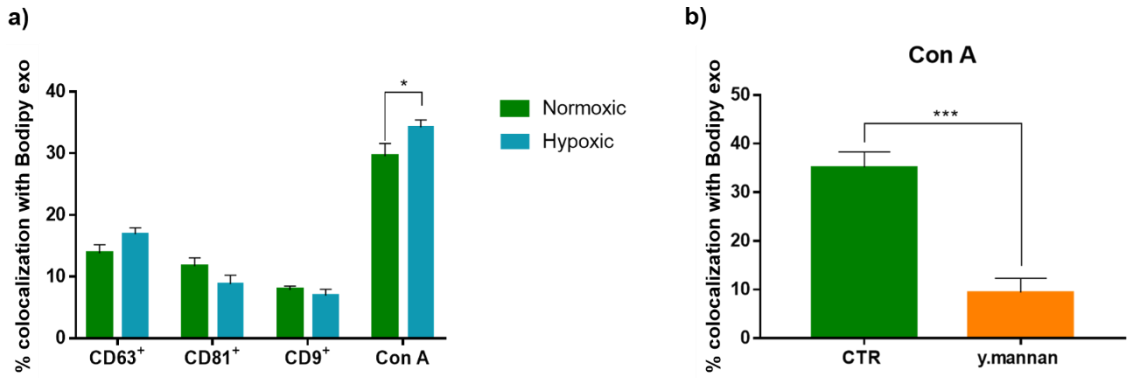

Figure 7 Analysis of protein and glycosylation profile. (a) Normoxic and hypoxic Bodipy exo have been incubated with antibodies anti-CD63 BV421, Anti-CD81 APC, anti-CD9 PE and with Con A conjugated with Alexa Fluor 647. Protein analysis shows that hypoxic condition doesn't changes in a significant way the tetraspanins expression. Hypoxic exosomes present a higher glycosylation than normoxic exo. Data are expressed as mean ± SEM (n=8). (**b)** Normoxic exosomes have been labeled with Con A in +/- y.mannan to observe the specific lectin binding to the exosomes. Data are expressed as mean ± SEM (n=6). Paired t test was performed to compare the % of colocalization of Bodipy exo with Con A in presence or absence of y.mannan. *p < 0.05, **p < 0.01, ***p< 0.001, ****p< 0.0001.

3.8 Characterization of immature Dendritic Cells (iDCs)

Following the characterization of Bodipy exo glycosylation profile, uptake experiments were performed on primary cells, in particular on immature dendritic cells (iDCs). iDCs, are known to express on their surface receptors similar to type C lectins (CLRs) that recognize different types of sugars (R. T. Lee et al., 2011; Robinson, Sancho, Slack, LeibundGut-Landmann, & Reis e Sousa, 2006). Here our aim was to demonstrate that highly mannosylated exosomes are internalized by antigen presenting cells (APCs) via the mannose receptor (MR/CD206). In order to perform uptake experiments, monocytes have been isolated from buffy coats and cultured in presence of IL-4 and GM-CSF for 7 days. Cells were then analyzed by Flow Cytometry (FC) to determine the main iDCs markers, and more specifically the percentage of expressed CD206 (Figure 8).

iDCs markers

	% of expression	
	Mean	SEM
CD14	2,0	0,4
CD1a	53,5	5,1
CD11c	4,1	1,6
CD209	71,2	3,6
HLA-DR	77,7	4,6
HLA-A2	37,0	6,1
CD80	62,3	4,7
CD86	14,6	2,5
CD83	5,2	0,8
CD206	**49,7**	3,8

Figure 8 iDC markers. After 7 days of incubation with IL-4 and GM-CSF, cells have been analyzed for the expression of principal iDCs markers by FC. Data are expressed as mean ± SEM (n≥10).

3.9 Bodipy exo internalization by immature Dendritic Cells

To demonstrate that Bodipy exo are specifically internalized via the MR uptake pathway, yeast mannan from Saccharomyces Cerevisiae (y.mannan), was used as competitor for the binding to the MR. Time-course experiment have been performed by using a fixed number of Bodipy exo incubated at 37°C. It is possible to observe that there was a significant inhibition of Bodipy exo uptake by y.mannan already at 30 minutes (Figure 9). This time point was chosen for the subsequent uptake experiments.

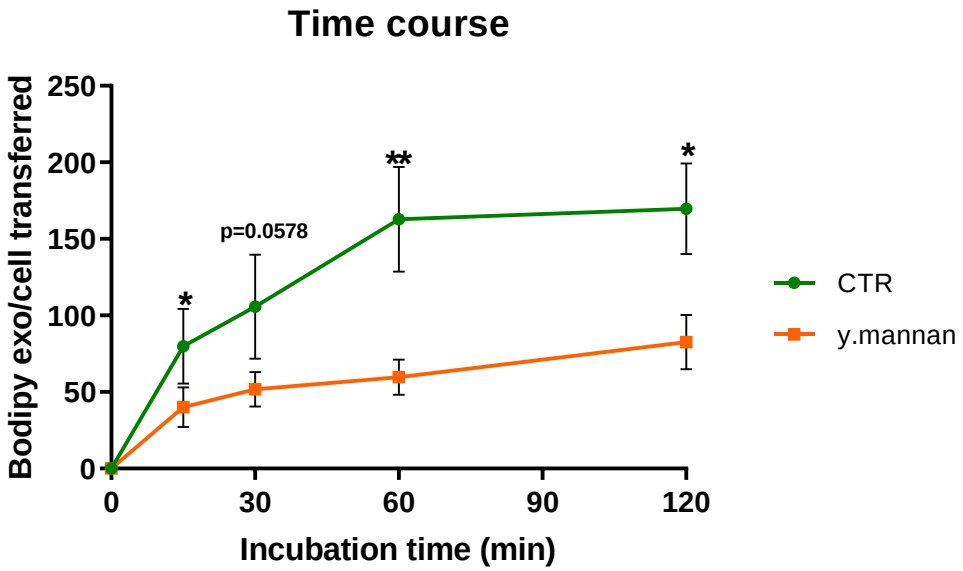

Figure 9 Time course of Bodipy exo internalization on iDCs. A fixed number of iDCs have been incubated with Bodipy exo for different time points at 37°C in Hank's Balanced Salt Solution. To determine the specificity of uptake by MR/CD206 we used yeast mannan a competitor of MR uptake. Cells were then analyzed by FC in the presence of the vital dye TO-PRO3 iodide. Data are expressed as mean ± SEM (n=7). Paired t test was performed to compare the number of exo internalized in presence or absence of y.mannan. *p < 0.05, **p < 0.01, ***p< 0.001, ****p< 0.0001.

A fixed number of iDCs have been incubated with an increasing number of normoxic or hypoxic Bodipy exo in presence or absence of y.mannan at 37°C for 30 minutes. Cells have been analyzed by FC. The analysis shows how Bodipy exo are specifically and very efficiently internalized by iDCs since y. mannan inhibits uptake by about 50%. Plateau is reached at a concentration of 150 Bodipy exo per cell. (Figure 10a).

To demonstrate the specificity of the internalization through CD206, binding experiments have been performed at 0 °C to inhibit the endocytosis mechanism. iDCs have been incubated with Bodipy exo on ice for 1 h in presence or absence of y.mannan, then were further incubated at 37°C for 30 minutes. It is possible to observe in Figure 10b the uptake of Bodipy exo is inhibited in presence of y.mannan but hypoxic Bodipy exo seem to be internalized via the MR more efficiently than normoxic exosomes.

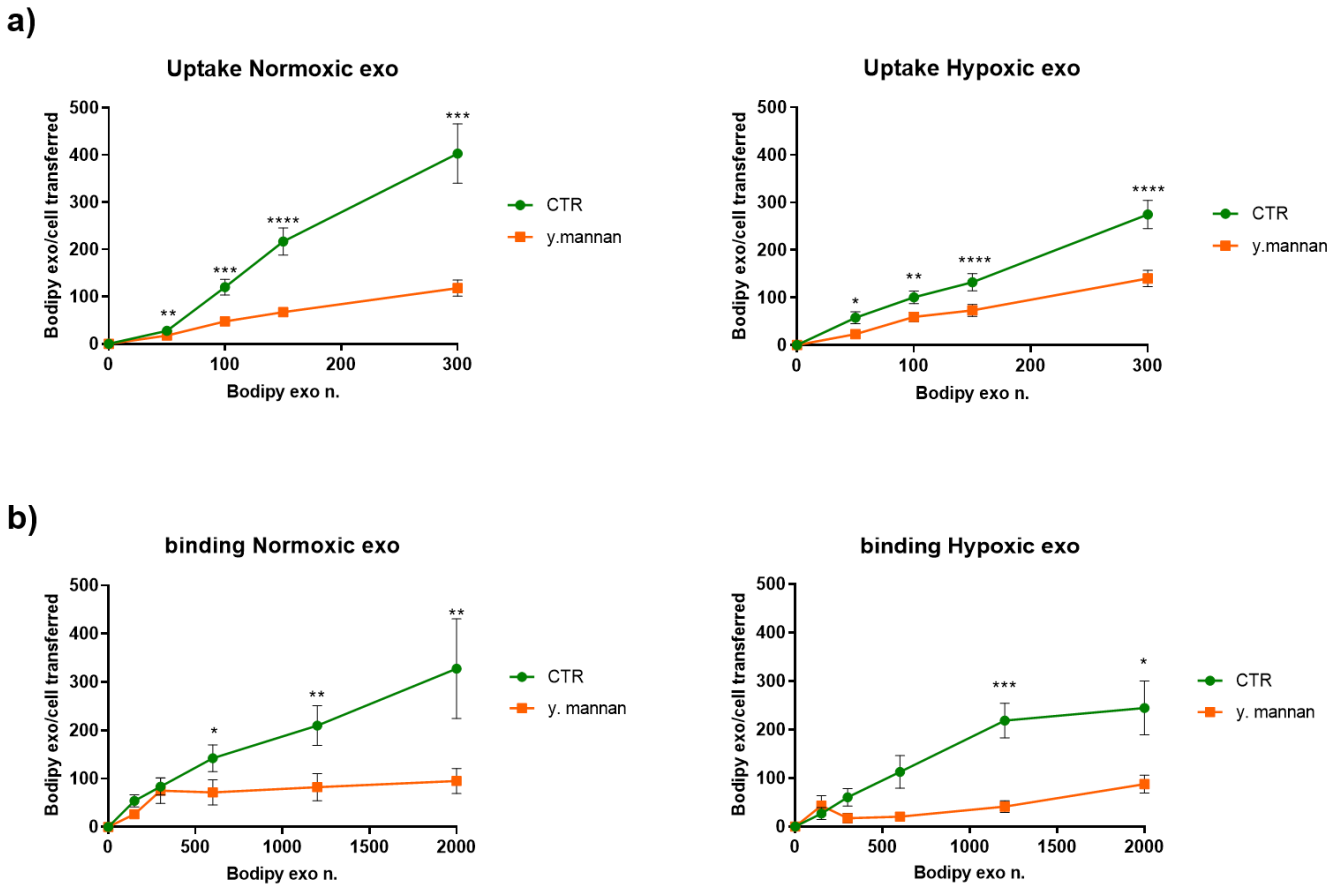

Figure 10 Bodipy exo internalization on iDCs. (a) iDCs have been incubated with normoxic or hypoxic Bodipy exo +/- y.mannan for 30 minutes at 37°C. FC analysis showed that all exosomes incubated with cells have been transferred and in presence of y.mannan there is an inhibition of 50% of the uptake. Data are expressed as mean ± SEM (n=40). (**b)** Both normoxic and hypoxic Bodipy exo bind specifically to iDC for 1 h at 4°C. Data are expressed as mean ± SEM (n=6). Paired t test was performed to compare the number of exo internalized in presence or absence of y.mannan. *$p < 0.05$, **$p < 0.01$, ***$p< 0.001$, ****$p< 0.000$

3.10 Bodipy exo are specifically internalized via the Mannose Receptor

The mannose receptor is a member of the C-type lectin (CLEC) family, which can bind and internalize a variety of endogenous and pathogen-associated ligands by recognizing mannose, fucose, or GlcNAc residues in a calcium-dependent manner (Ezekowitzt, 1998; L. Martinez-Pomares, 2012; Philip Stahl, 1980; van der Zande et al., 2021). MR is a Ca_2 dependent receptor. To better demonstrate that exosomes are internalized by iDCs via MR, uptake experiments were performed in presence of 2mM EDTA, a calcium chelanting agent, at 37°C for 30 minutes. The analysis showed that in presence of EDTA there was an inhibition similar to that caused by y.mannan (Figure 11a). To demonstrate that Bodipy exo are not internalized by other endocytosis mechanisms, such as micropinocytosis or phagocytosis, we used Cytochalasin D, a drug that acts by inducing the depolymerization of the actin cytoskeleton that selectively block endocytosis of membrane bound ligands that acts by disrupting actin filaments. Data showed that this inhibitor alone doesn't inhibit Bodipy exo uptake, while by combining the effect of Cytochalasin D and y.mannan a complete inhibition was obtained. This result suggest that only the Mannose Receptor is involved in the Bodipy exo internalization (Figure 11b). An additional confirmation was obtained through uptake experiments on cells that don't express MR, particularly Peripheral Blood Mononuclear Cells (PBMCs). The experiment was conducted under the same conditions as with iDCs, and no internalization of Bodipy-labeled exosomes was observed, as expected (Figure 11c).

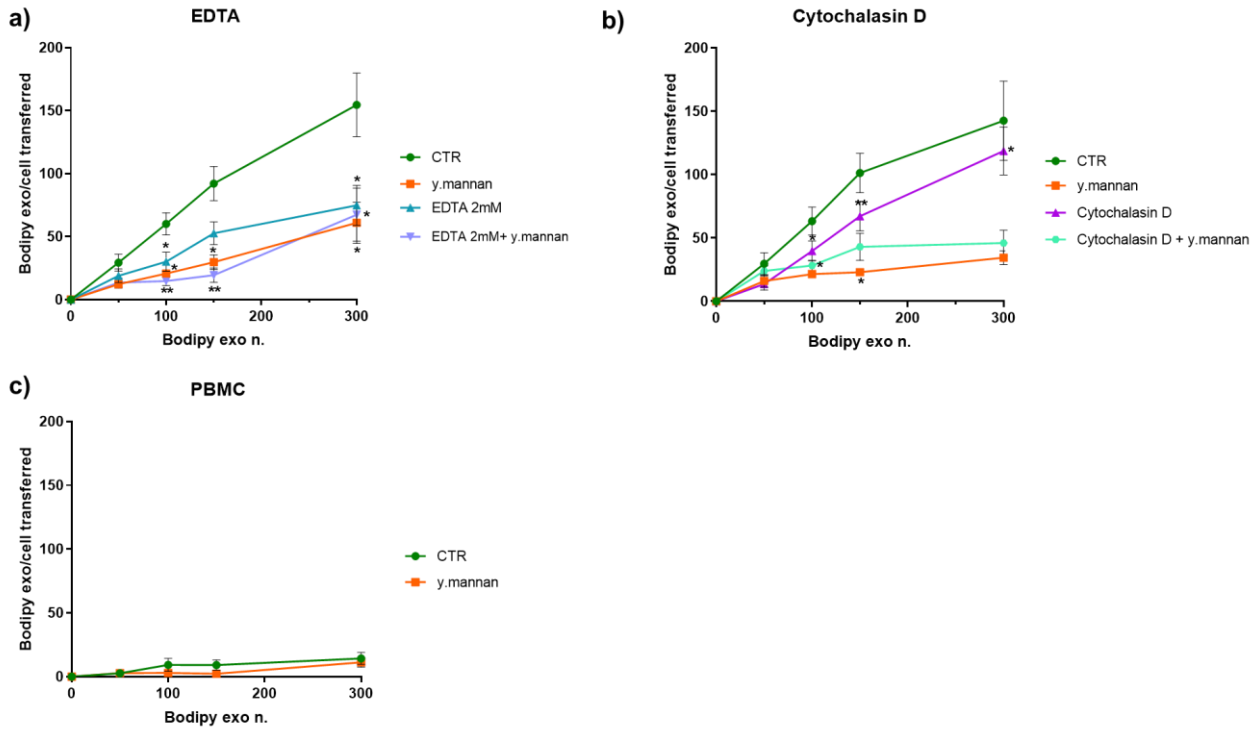

Figure 11 Bodipy exo internalization is mannose Receptor dependent. (a) EDTA, a chelating calcium agent, inhibit Bodipy exo uptake via MR like the effect of y. mannan alone. **(b)** In presence of Cytochalasin D it was observed a slightly inhibition endocytosis, while the combination of Cytochalasin D and y.mannan inhibit Bodipy exo internalization underling the role of MR in this process. **(c)** PBMC (Peripheral Blood Mononuclear Cell) don't express MR, so they have been used as negative control. Result shows that there is no internalization of Bodipy exo. Uptake experiments were performed for 30 min at 37°C. Data are expressed as mean ± SEM (n≥5).

3.11 Study of Bodipy exo distribution on iDCs

Bodipy exo internalization has been observed also by images acquired in fluorescence mode. iDCs have been incubated with normoxic Bodipy exo for 30 min in presence or absence of y.mannan. Images showed green spots inside cells at the cytoplasmatic level that presumably are internalized Bodipy exo. In presence of y.mannan there is a less or almost no internalization of Bodipy exo. This observation confirms all the results previously showed(Figure 12).

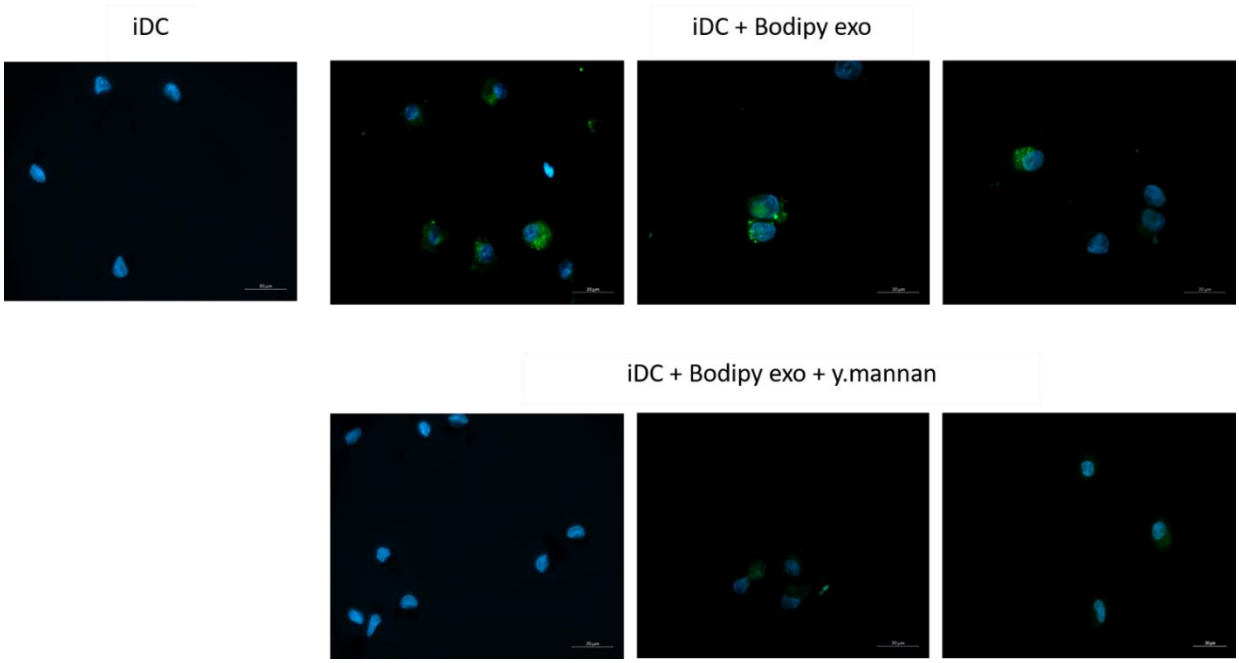

Fig. 12 Bodipy exo distribution on iDC. Bodipy exo have been incubated with iDC for 30 min at 37°C +/- y.mannan. Bodipy exo seem to be localized at cytoplasmatic level and in presence of y.mannan the internalization is almost null. Images are representative of 3 indipendent experiments.

3.12 Exosomes induce mature dendritic cells differentiation

The next step was to study the possible role of normoxic or hypoxic exosomes to induce iDCs differentiation in mature dendritic cells (mDCs) capable of presenting the antigen. After taking up pathogens, infected cells, or apoptotic cells, DCs process antigens derived from these particles into peptides and load them on major histocompatibility complex (MHC) class I or MHC class II molecules (Ariel & Sebastian, 2007). Antigen loaded on MHC class I are presentend to CD8+ T through a process referred to as cross-presentation (Andres, Fiorella, Gamelas, & Sebastian, 2016). To determine if exosomes can induce differentiation into mDC, compared variations in the expression of dendritic cell markers were compared by incubating iDC with normoxic or hypoxic exosomes in presence or not of y.mannan (indicated as a light colour) by using as control cells treated with Lipopolysaccharides (LPS), known to induce differentiation into mDC. Expression analysis of mDC markers was performed after 48 h of incubation. The main markers taken into consideration are CD80 and CD86, as they are involved in the activation of T lymphocytes, CD83 and CD206. In Figure 13 is possible to observe a significant increase in CD80, CD86, and CD83 both with normoxic and hypoxic exosomes as well as with LPS between 0 hr (immature DCs) and 48 hr. An important evidence is that, in the case of CD83 the presence of y.mannan together with normoxic exosomes slows down the increase in expression of this marker at 48 hr, while there are no differences observed with LPS and hypoxic exosomes. Also in the case of the CD80, the presence of y.mannan slows down the effect of normoxic exosomes on the expression of this marker. The most important effect regards the expression of CD206. Analysis showed that at 48 hr normoxic exosomes induce a significant downregulation of MR inhibited by the presence of y.mannan, while hypoxic exosomes maintain an high expression of this receptor. These results are extremely encouraging, as further demonstration that the internalization of exosomes by iDCs occurs via CD206.

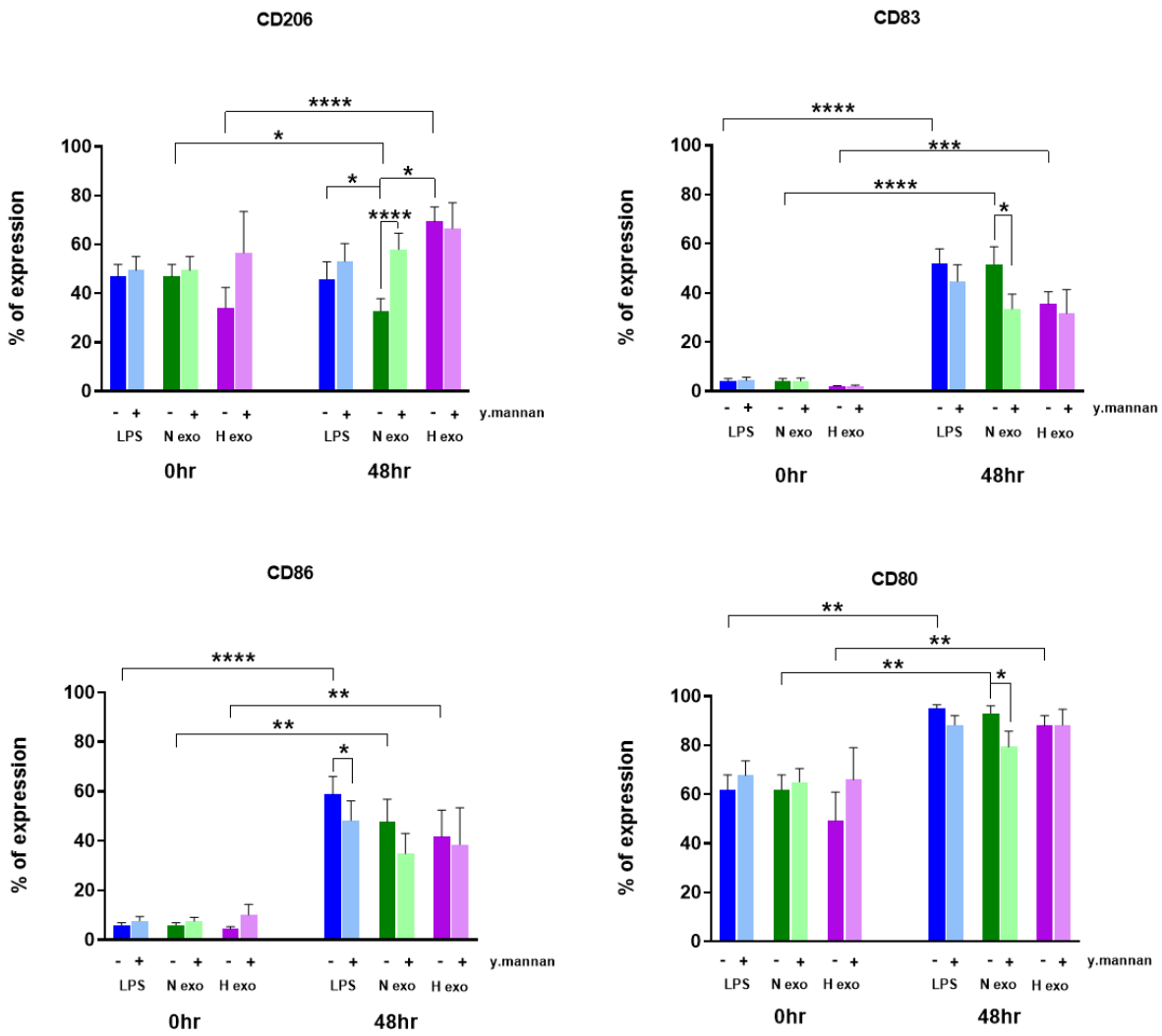

Figure 13 Exosomes induce iDCs differentiation in mature DC. iDCs have been incubated for 48 hr in presence of LPS, normoxic exosomes (N exo) or hypoxic exosomes (H exo) +/- y.mannan. After treatment, cells have been analyzed for the expression of mature DC markers Data are expressed as mean ± SEM (n≥14). Paired t test was performed to compare two groups. *p < 0.05, **p < 0.01, ***p< 0.001, ****p< 0.0001.

The supernatant of iDC cells treated with normoxic exosomes and LPS were analyzed by ELISA for the presence of TNF-a and IL12-p70, two cytokines released during the inflammatory response by mature dendritic cells. Results showed that exosomes induce a major release of TNF-α by dendritic cells compared to LPS (Figure 14a). The analysis of IL12-p70 is particularly interesting, as there is a significant release in the presence of LPS. However, also with exosomes, it is possible to observe the release of this cytokine by dendritic cells. (Figure 14b).

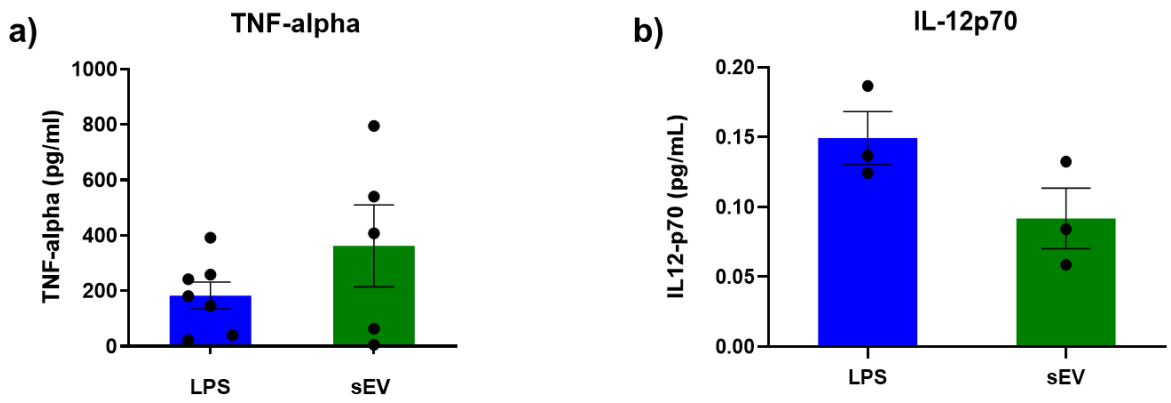

Figure 14 Analysis of cytokines released by DC. Supernatant of cells treated with LPS or normoxic exosomes for 48 h have been analyzed by ELISA test for (**a)** TNF-alpha and (**b)** IL12-p70 cytokines. Data are expressed as mean ± SEM (n=3).

4. Discussion

The role of exo in cell-to-cell communication and their possible clinical applications are a major subject of interest, especially in recent years. However, the difficulties encountered in the separation of exosomes from other types of Extracellular Vesicles (EVs) represent a problem, not only for the study of the functions of these nanovesicles and their use in clinic, but also various aspects relating to the mechanisms of biogenesis and interaction with the recipient cells are not fully elucidated (Dixson, Dawson, Di Vizio, & Weaver, 2023; Gurung et al., 2021; Teng & Fussenegger, 2020).

With the aim to develop an effective strategy for labeling exosomes that could be distinguished from microvesicles or ectosomes we previously reported a novel methodology by using Bodipy C16, a fluorescent palmitic acid analogue. We have already shown that Bodipy C16 is mainly metabolized into constitutive lipids that become part of the sEV membrane bilayer producing fluorescent sEV that can be readily counted by FC (Coscia et al., 2016). In the first part of this project, we provide evidence that the population of fluorescent sEV released from Bodipy C16 labelled cells is a discrete subpopulation of exosomes originating from an intracellular pathway. Cellular uptake of Bodipy C16 is very rapid and we here show that the probe is promptly metabolized to polar lipids and very little free Bodipy C16 can still be detected as early as 30 minutes of chase. Fluorescent exosomes, regardless of the secretion time, contain Bodipy lipids almost completely in the form of phospholipids with very little residual unmetabolized Bodipy C16. Newly formed Bodipy lipids can be tracked in phospholipid biosynthesis sites such as the ER and mitochondria, and in definite intracellular organelles where they colocalize with established markers of exosomes such as LBPA, CD63 and CD9 but not with CD81 that in melanoma cells, as also reported by others for other cell types (Fordjour et al., 2022) we found was mainly localized on the plasma membrane. Absence of colocalization of Bodipy with the lectin Con A used to label the plasma membrane was a further proof that Bodipy

phospholipids are excluded from the plasma membrane. In order to establish a more direct relationship between fluorescent exosome secretion and the intracellular route of ILV formation, we conducted a detailed analysis of the physicochemical and molecular characteristics of Bodipy-labeled exosomes. The fluorescence labeling procedure we developed represents a significant improvement over current methodologies used for generic labeling of sEV. Despite recent advancements in achieving high-resolution quantitative and qualitative analysis of cell-derived vesicles using FC (Higginbotham et al., 2016; Morales-Kastresana et al., 2019; Pospichalova et al., 2015), it is important to note that all the dyes utilized in these approaches are nonspecifically incorporated into ultracentrifugation pellets, which consist of heterogeneous populations of vesicles. Consequently, this poses a challenge in accurately quantifying and characterizing the vesicles. Our methodology enabled us to track fluorescent vesicles originating from the metabolic site of phospholipid synthesis that could be accurately monitored after isolation using current protocols involving differential centrifugation combined with iodixanol density gradient floatation. Bodipy exosomes separated as a discrete peak (1.07-1.08 g/ml), positive for the exosome markers CD63, CD81, CD9, Alix, and Syntenin 1. In contrast, CFSE-labeled sEV displayed an additional fluorescent peak at a higher density (>1.16 g/ml), which only in part was detergent soluble suggesting the presence of non-detergent soluble aggregates. Annexin 1, identified as a specific marker for ectosomes shed from the plasma membrane (Jeppesen et al., 2019), was present in the same fractions as Bodipy-labeled exosomes. This finding aligns with previous reports indicating that Annexin 1 can be found in both Exo-S and Exo-L preparations (Zhang et al., 2018). Given that the ratio of Bodipy-labeled exosomes to total sEV in our samples prepared from 24 h chase conditioned media is 1:10, it is plausible that vesicles of different origins, such as exosomes and ectosomes, may coexist within the density gradient fractions corresponding to the fluorescent peak.

Tetraspanins proteins, particularly CD63, CD81, and CD9, play a critical role in vesicle biogenesis and cargo sorting and have been widely used as markers for

exosomes although it is now evident that these tetraspanins are also expressed on ectosomes and other subtypes of sEV (Fordjour et al., 2022; Kowal et al., 2016; Mathieu et al., 2021; Zhang et al., 2018). Recent advances in imaging flow cytometry that enable the multiparameter characterization of single EV combined with novel EV labeling strategies, now allow us to investigate the phenotypic heterogeneity within exosomes and other EV populations with high precision (K. Lee et al., 2018). Nevertheless, the exploration of heterogeneity within tetraspanin-positive EV subpopulations is currently limited to a few studies that primarily rely on bulk vesicle preparations (Ricklefs et al., 2019; Woud et al., 2022). We exploited the unique features of our methodology to accurately determine the tetraspanins surface profiles on Bodipy-labeled exosomes. Our data indicate that CD63+ Bodipy labeled exosomes are the most abundant followed by those positive for CD81. In contrast, CD9-positive exosomes represent a minor fraction, despite observing a higher degree of intracellular colocalization between Bodipy lipids and CD9 compared to CD81. This suggests that although there is a significant intracellular association between CD9 and Bodipy lipids, CD9 may be selectively sorted or retained within the cell, resulting a lower abundance of CD9+ Bodipy labeled exosomes. Double positive CD63+/CD81+ are also present while CD63+/CD9+ exosomes were detected in smaller proportions. The differential sorting and release mechanisms of tetraspanins may contribute to the observed variations in their presence on exosomal membranes. It has been proposed that exosomes are primarily enriched in CD63, which serves as a late endosome and MVB marker, while EVs bearing only CD9 or CD81, without CD63, may not form within endosomes (Mathieu et al., 2021; Zhang et al., 2018). We cannot rule out the possibility that single-positive CD81+ Bodipy-labeled exosomes may include small vesicles directly budded from the plasma membrane, where CD81 is predominantly localized in Mel501 cells. However, in our study, we did not observe colocalization of CD81 with Bodipy lipids on the plasma membrane, despite observing it at steady state. A potential explanation for the observed discrepancy has already been raised in previous work in a human B-cell line where it has been

observed that CD81 is the most highly enriched protein in exosomes, even though it is primarily localized to the plasma membrane (Escola et al., 1998). This discrepancy was attributed to the inefficient detection of intracellular CD81 molecules by the relevant antibody, potentially due to epitope masking. Our data also show that despite the significant intracellular colocalization of CD9 with Bodipy lipids, CD9+ Bodipy-labeled exosomes were present in lower percentage compared to other tetraspanin-positive exosomes suggesting an active mechanism of intracellular Bodipy lipids sorting. However, the absence of a particular tetraspanin marker does not necessarily indicate the mode of sEV biogenesis, as some sEV may lack certain markers despite forming in endosomes.

By applying a nanoFACS sorting strategy we obtained a pure subpopulation of exosomes that could be further examined by electron microscopy (TEM). The sorted subpopulation of Bodipy exosomes had a mean size of 80 nm significantly smaller that the bulk of sEV present in the presorted samples analyzed by both SEM and NTA. The size of Bodipy labelled exosomes coincides with the Exo-S subpopulation of exosomes reported recently as the most likely bona fide/canonical exosomes (Zhang et al., 2018). Furthermore, immunogold staining revealed the colocalization of the Bodipy moiety and CD63 within the same vesicle, providing conclusive evidence for the exosome nature of the Bodipy-labeled vesicles.

By studying the release dynamics of Bodipy exosome release, we determined that they accounted for approximately 20% of the total sEV secretion. The kinetic profile of Bodipy exosomes overlapped with that of total sEV for the first 6 hr of the chase period. After this time, it is presumed that the intracellular reservoir of Bodipy lipids was depleted, although residual fluorescence associated with the cells could still be detected. This observation suggests that Bodipy-derived phospholipids might be incorporated into other intracellular membranes that do not contribute to the formation of ILVs. In conclusion, our study introduces an innovative methodology for metabolically labeling fluorescent exosomes using a fluorescent palmitic acid that

is readily internalized by cells and is transformed into phospholipids which will form part of the lipid bilayer of the secreted exosomes. The strong evidence presented in this study confirms that the Bodipy-labeled sEV are indeed exosomes (Bodipy exo).

Exosomes, released by both normal and tumor cells, are emerging as key mediators of intercellular communication with an important role in modulating immune responses. However, it remains unclear whether these vesicles secreted by donor cells are selectively or non-selectively incorporated into recipient cells. Even if there are several internalization mechanisms, it is still not known if they are equally effective in targeting specific signaling pathways involved in tumor progression and/or immune escape (Martins et al., 2021; Mathieu et al., 2019; McKelvey et al., 2015; Mulcahy et al., 2014). Recent studies have shown that exosomes are coated with high mannose glycans on their surface (Kondo et al., 2022; Lin et al., 2020; Martins et al., 2021). The glycosylation profiles of both cells and exosomes can be altered in hypoxic conditions, such as those found in the tumor microenvironment (Harris, 2002; Jing et al., 2019; Ryan P. McNamara, 2021). Tumor cells change their metabolism from oxidative phosphorylation to glycolysis, leading to changes in glycosylation patterns. We wanted to evaluate the specific uptake mediated by the MR of exosomes secreted under normoxic or hypoxic condition. First of all, we evaluated if Bodipy exo, released from A375/M cells cultured under normoxic (21% O_2) or hypoxic (5% O_2) conditions, presented differences in the expression of tetraspanins, CD63, CD81 and CD9. FC analysis showed that protein expression was not altered in hypoxic conditions, but interestingly glycosylation was different between hypoxic and normoxic exo. By using Concanavalin A, a lectin that specifically binds α-D-mannosyl and α-D-glucosyl residues, we observed that the reduction of oxygen induced a significant increase of glycosylation in exosomes, thus confirming what is reported in literature (Amanda P.B. Albuquerque1 & A. Reis, 2018).

Dendritic cells (DCs) are the principal player in the TME and that function as a bridge between the innate and adaptive immune systems. DCs are involved in immune activation and the recruitment of immune effector cells and pathways within the TME (Tran Janco, Lamichhane, Karyampudi, & Knutson, 2015). They are also important for antigen presentation to T cells, making them a preferential target for infiltrating T cells (Tran Janco et al., 2015). Dendritic cells, in particular immature dendritic cells (iDCs) express on their surface the Mannose Receptor (MR/CD206), so in the second part of this project we wanted to investigate the specific exosomes internalization by MR. We used the yeast mannan (y.mannan), from Saccharomyces Cerevisiae, as competitor for the binding with the MR. Usually uptake experiments are performed for 24 h, so we made time course experiments by incubating a fixed number of Bodipy exo with iDCs for different time points. From our results it is possible to observe that already at 30 minutes y.mannan inhibit Bodipy exo internalization almost by 50%, suggesting that exosomes uptake via the MR is a specific mechanism. We then performed uptake experiments on iDCs incubating an increasing number of normoxic or hypoxic Bodipy exo at 37°C for 30 minutes in presence or absence of y.mannan. Since our exosomes are fluorescent, we are able to quantify the number of Bodipy exo incubated and transferred per cells. Uptake analysis showed that both normoxic and hypoxic exosomes have been transferred to the iDCs and in presence of y.mannan there was a 50% inhibition of internalization already visible at 150 Bodipy exo per cell suggesting that this mechanism is extremely specific and that MR/CD206 play an important role in this process. To better demonstrate that the MR is the principal mechanism of exosomes internalization, we performed binding experiments to better analyze the nonspecific binding. Both normoxic and hypoxic Bodipy exo have been added to iDCs at 4°C for 1h and then incubated at 37°C for 30 minutes. As it is possible to observe in Figure 10b, even in this case we observed an inhibition by almost 50% in presence of y.mannan, but hypoxic Bodipy exo seems to be more efficiently internalized via the MR.

The MR is a calcium-dependent receptor (Ezekowitzt, 1998; L. Martinez-Pomares, 2012; van der Zande et al., 2021), we decided to perform uptake experiments in presence of EDTA, a calcium-chelating agent. Chelating agents are substances that can form coordination complexes with metal ions by binding to them through multiple coordination sites. In the case of EDTA, it has four carboxylic acid groups (-COOH) and two amine groups (-NH2) that can form strong bonds with metal ions, including calcium (Ca2+). Our results showed that in presence of EDTA Bodipy exo uptake is inhibited such as y.mannan, thus confirming our previously data.

To inhibit endocytosis mechanism we used Cythocalasin D, a drug that acts by inducing the depolymerization of the actin cytoskeleton that selectively block endocytosis of membrane bound ligands (Kuhn et al., 2014; Rotsch & Radmacher, 2000). We observed a slightly inhibition of endocytosis, while by combining Cytochalasin D and y.mannan we observed an inhibition of Bodipy exosomes internalization suggesting that is the only MR involved in this process. Cytochalasin D is used to study actin-dependent uptake mechanisms, that is, phagocytosis and micropinocytosis, mechanisms that are principally attributed to macrophages, so probably the inhibition of Bodipy exo internalization via endocytosis process could be evident with the M2-type macrophages (M2 Φ). Overall, Cytochalasin D primarily affects the actin cytoskeleton and has various effects on cellular processes such as adhesion, spreading, stress fiber disassembly, and cytokine expression. While it may indirectly affect the MR through its impact on the actin cytoskeleton, there is no direct evidence of a specific interaction.

Moreover, no internalization of Bodipy exo was observed by Peripheral Blood Mononuclear Cell (PBMC) not expressing the MR/CD206, confirming our results.

Once we demonstrated that the mannose receptor is the specific mechanism for exosome internalization, our next aim was to investigate the potential role of these vesicles in inducing dendritic cell maturation. We also sought to determine whether the MR/CD206 pathway plays a role in this process. To do this, iDCs have been

incubated with either normoxic or hypoxic exosomes, in the presence or absence of y.mannan, for 48 hr. As a control, we used lipopolysaccharide (LPS). We focused on mature dendritic cells markers (mDCs), specifically CD80, CD86, CD83 and also on CD206. As Figure 13 illustrates, both normoxic and hypoxic exosomes were equally effective as LPS in inducing maturation of iDCs, as indicated by the increased expression of CD86, CD80, and CD83. In contrast, the MR/CD206 appeared to be downregulated only in response to normoxic exosomes when they are taken up via the MR mechanism. Hypoxic exosomes did not induce the downregulation of CD206. This observation led us to hypothesize that these vesicles may play a role in the tumor microenvironment, potentially contributing to the maintenance of an anti inflammatory state that facilitates tumor growth and inhibits antigen presentation. Furthermore, our results indicated that the expression of CD83 and CD80, but not CD86, appeared to be affected by the MR-mediated uptake of normoxic exosomes, and this effect was influenced by the presence of y.mannan. Moreover we analyzed by ELISA test the level of TNF-α and IL 12-p70 released in the supernatant of cells treated with LPS and normoxic exosomes after 48 h. These preliminary data would seem to suggest that exosomes could have an important role in the immune modulation response. Future experiments will focus on cytokines secretion profiles of exosomes treated iDCs and miRNA profiles of normoxic and hypoxic exosomes.

5. Methods

5.1 Cell lines and culture

The human melanoma cells Mel 501 was cultured in RPMI 1640; the human melanoma cells A375/M and Me665/1 (Me665), the human embryonic kidney 293T (HEK293T) and the human cervical adenocarcinoma HeLa cells, were cultured in Dulbecco's modified Eagle's medium. All media were supplemented with 10% heat-inactivated fetal bovine serum (FBS), 100 units/ml penicillin, 100 μg/ml streptomycin and 2 mM L-glutamine (complete media). Additional 1% MEM Non Essential Aminoacids were added to A375/M cell media. All media and supplements were from Euroclone. When required for Nanoparticle Tracking Analysis (NTA) or CFSE staining of sEV, FBS was replaced with Exosome Depleted FBS (Euroclone) (EV depleted medium). Cell lines were grown at 37°C, under 5% CO2, in humidified incubators and routinely tested for mycoplasma contamination using the Mycoplasma PCR Detection Kit (ABM, #G238). All cell lines are commercially available (ATCC) with the exception of Me665/1 stabilized from surgical specimen at Istituto Nazionale Tumori (Milan, Italy) (Felicetti et al., 2008).

5.2 Cells and sEV labelling

BODIPY FL C16 (Bodipy C16) (4,4-Difluoro-5,7-Dimethyl-4-Bora-3a,4a-Diaza-s-Indacene-3-Hexadecanoic Acid (ThermoFisher, #D3821) or Palmitic acid (Sigma, #P0500) were complexed with fatty acid-free bovine serum albumin (BSA), (Sigma, #A8806) as described previously (Coscia et al., 2016). To isolate sEV, 60-70% confluent monolayers of cells in exponential growth were incubated with 7 μM Bodipy C16 or palmitic acid at 37 °C for 4 or 5 h, or for the times indicated in the figure legends, in medium containing antibiotics and glutamine and supplemented with 0.3% FBS (cell labeling medium). Cells were washed twice with Hank's balanced salt solution (HBSS) containing 0.1% (w/v) fatty acid-free bovine serum albumin (H-BSA) to remove excess probe and further incubated in complete culture medium. The conditioned medium was either immediately processed for EV isolation or stored at

4°C for up to one week. Cells were detached from the plates with trypsin/EDTA, and their viability was assessed by Trypan Blue exclusion. The sEV release per cell was calculated for experiments with cells showing ≥ 75% viability. To determine the total cell-associated fluorescence in pulse-chase experiments, cells were detached at different time point, washed with PBS and fixed with 4% paraformaldehyde in PBS for 30 min in the dark at room temperature (RT). Next, cells were detached at different time points and the fluorescence (Mean Fluorence Intensity, MFI) was determined by FC. To obtain sEV for generic fluorescent labeling, cells were treated as in pulse chase experiments with the difference that the complete medium was replaced by EV depleted medium. Freshly pelleted 100K sEV from conditioned medium were labeled with 10 μM 5-(and-6)-Carboxyfluorescein Diacetate Succinimidyl Ester (CFDA-SE, hereinafter referred to as CFSE) (ThermoFisher) for 30 min at RT in the dark. The reaction was stopped by adding 100 mM L-glutamine, and the number of fluorescent EVs was quantified by FC.

5.3 sEV isolation by differential ultracentrifugation

Conditioned medium was collected 24 h after pulse media exchange or at the indicated chase time intervals and serially centrifuged at 2000*g* for 20 min at 4°C to discard cells and large debris. The supernatant was centrifuged at 10,000*g* for 20 min at 4°C for microvesicles and other debris. The supernatant was then ultracentrifuged 100,000*g* for 90 min at 4°C and the pellet (100K pellet) was washed in 12 ml of PBS and centrifuged again at 100,000g in a SW41 Ti swinging bucket rotor (Beckman Coulter). Pellets were resuspended in PBS.

5.4 NanoFACS analysis of Bodipy sEV

Quantification of fluorescent Bodipy sEV was evaluated as described (Coscia et al., 2016) with a conventional non-customized CytoFLEX LX flow cytometer (Beckman Coulter) by exploiting their fluorescent emission. To establish the region containing the sEV, threshold and gain values were initially defined on the appropriate fluorescent channel with a band pass of 525/40 by using fluorescent beads of known sizes ranging from 100 to 900 nm (Megamix Plus FSC/SSC, BioCytex, #7802/7803).

The instrument was then set to include fluorescent size reference beads smaller than 100 nm. To obtain the number of sEV, the Cytoflex LX instrument utilized a sample peristaltic pump capable of calibrating the volume delivery of the sample, allowing for absolute EV counts without the need for bead-based calibration.

5.5 NanoFACS sorting of Bodipy sEV

To sort the Bodipy-positive population of sEV, we utilized a MoFlo Astrios-EQ instrument equipped with four lasers (405, 488, 561 and 640 nm) and set up as described in (Lanna et al., 2022). In detail, the threshold value was applied on the side scatter of the 488 nm blue laser (B-SSC. Plotting B-SCC Height signal versus B-SCC Width signal allowed the exclusion of vesicle aggregates and other background noise from the target population. In order to determine the appropriate threshold value for sorting the Bodipy-positive population of sEV, we utilized fluorescent size reference beads (110 nm to 1300 nm size beads, ApogeeMix, #1493). PBS and unlabeled sEV were used to assess the background noise and the not fluorescent signal, respectively (Figure 6a, dot plot on the left). A gating strategy has also been applied to eliminate aggregated vesicles and background noise by plotting B-SCC Height signal versus B-SCC Width signal. The cells sorter is also equipped with inline sheath filter with 40 nm pore size to decrease the background noise. Finally, the flow rate was settled to reduce the electronic and the PBS background noises to less than 300 events/sec. Acquisitions, cell sorting, and analyses were performed by using the Summit 6.3.1 software (Beckman Coulter).

5.6 Nanoparticle tracking analysis

EVs secreted by the same initial number of cells untreated or treated with Palmitic Acid or Bodipy C16, have been quantified by Nanoparticle tracking analysis (NTA) performed with a NanoSight NS300 system (Malvern Instruments, UK). Camera level was set at 16 for all recordings. Camera focus was adjusted to make the particles appear as sharp individual dots. Five 60-second videos were recorded for each sample with a delay of 7 seconds between each recording at a fixed temperature of

25 °C. Analysis was performed with NTA 3.4.4 software. Detection threshold was set at 5 and other settings were kept at default.

5.7 Iodixanol density gradient separation

Bodipy sEV (100K pellets) were bottom loaded in a discontinuous iodixanol gradient (35% (w/v), 25% (w/v), 15% (w/v) and 5% (w/v)) made by diluting OptiPrep (60% (w/v)) iodixanol (Sigma-Aldrich, # D1556) with 60 mM Tris-HCl (pH7.4), 0.25 M sucrose, 1 mM of EDTA from the bottom to the top of an open-top polypropylene tube (Beckman Coulter, #328874). The gradient was centrifuged for 16 h at 33,000 RPM at 4°C (SW60 rotor, Beckman Coulter). A total of 13 fractions of 330 μl were manually collected from the top of the gradient and fraction density was assessed with a refractometer (Carl Zeiss). Bodipy sEV present in each fraction have been quantified by FC.

5.8 High Performance Thin Layer Chromatography (HPTLC)

Lipids from cells and exosomes were extracted in CHCl3/MeOH according to the Folch method (Folch, Lees, & Stanley, 1957). The extracted lipids were then resuspended in a small volume of 2:1 (v/v)CHCl3/MeOH and layered onto Silica gel 60 F_{254} plates (Merck, Darmstadt, Germany). For the separation of neutral lipids, a mixture of 70:30:1 hexane/ethyl ether/acetic acid was used, while for the separation of phospholipids, a mixture consisting of chloroform/methanol/acetic acid/water with a 50:37.5:3.5:2 (v/v) ratio was employed. The fluorescent lipid species were visualized using a Typhoon 9200 scanner (Amersham Biosciences, Little Chalfont, UK). 10 μg each of the following standards were used: lyso(bis)phosphatidic acid (LBPA), phosphoethanolamine (PE), phosphatidilcholine (PC), phosphatidilserine (Echelon Biosciences, Salt Lake City, UT, USA); phosphatidylinositol (PI), diacylglycerol (DAG), triacylglycerol (TAG), cardiolipin (CL) (Avanti Polar Lipids, Alabaster, AL, USA); cholesterol (chol)((Sigma-Aldrich, Saint Louis, MO, USA). Lipid standards were detected with 3% copper acetate solution in 8 % phosphoric acid and subsequent heating for 10 min at 120 °C.

5.9 Confocal Microscopy

To evaluate Bodipy C16 distribution, cells were seeded on 12 mm round coverslips in 24-well plates at a density of 80,000 cells/well the day prior to experiments and then incubated with 1 μM Bodipy C16 in cell labeling medium for 2 h at 37°C. Subsequently, cells were washed twice with ice cold H-BSA and then were fixed for 30 min with 4% paraformaldehyde in PBS at RT and stained with DAPI (Sigma, # F6057) to visualize nuclei. For colocalization experiments with mitochondria and lysosomes, Mel501 cells on coverslips were incubated with 200nM MitoTracker Deep Red or 50 nM LysoTracker Deep Red. MitoTracker incubation started 10 min before adding 1 μM Bodipy FL C16 whereas LysoTracker was added simultaneously. Incubation was carried out for 15 and 30 min after Bodipy C16 addition. Cells were then washed with PBS, fixed and mounted with DAPI as described above. For immunocolocalization experiments, cells were pulsed with 1 μM Bodipy C16 for 2 h at 37°C and washed twice with ice cold H-BSA. Cells were then fixed with 4% paraformaldehyde in PBS for 30 min at RT and permeabilized with 0.1% (w/v) saponin (Sigma) in PBS. Following blocking in PBS supplemented with 0.1% (w/v) saponin and 2.5% (w/v) BSA (blocking buffer), cells were incubated with primary antibodies diluted 1:100 in blocking buffer for 2 h at RT. Next, cells were washed twice with 0.1% (w/v) saponin in PBS for 10 min and successively incubated for 1 h at RT with secondary antibodies diluted 1:500 in blocking buffer. Cells were mounted with DAPI, as described above. For plasma membrane labelling, cells pulsed for 2 h with1 μM Bodipy C16 and washed twice with ice-cold H-BSA were incubated with 50 μg/ml Concanavalin A (Con A) on ice for 30 min. Cells were the washed with PBS, fixed and mounted with DAPI as described above. Images were acquired on a Zeiss LSM 900 confocal microscope using a 63X objective. At least 20 fields were captured for each condition, and these were representative of at least 3 independent experiments. The percentage of colocalization was calculated using Zen Blue software by dividing the pixels in the colocalized region for Bodipy C16 pixels. Antibodies and reagents for immunofluorescence were: MitoTracker Deep Red FM

(Invitrogen, #M22426), LysoTracker Deep Red, (Invitrogen, #L12492), Con A Alexa Fluor647 (Invitrogen, #C21421), mouse anti-Phalloidin TRITC (ECM Biosciences, #PF7551), mouse anti-BMP (Echelon, #Z-SLBPA), mouse anti-CD63 (BD Bioscience, #556019), mouse anti-CD81 (BD Bioscience, #555675), mouse anti-CD9 (Santa Cruz Biotechnology, #sc-13118), mouse anti-GM130 (BD Bioscience, #610822), mouse anti-Calnexin (BD Bioscience, #610524), goat anti-Calregulin (Santa Cruz Biotechnology, #sc-6467), goat anti-mouse AlexaFluor555 (Invitrogen, #A21424) and donkey anti-goat AlexaFluor 594 (Invitrogen, #11058).

5.10 Western Blot

EV proteins were separated by 10 or 12% sodium dodecyl sulphate (SDS) polyacrilamide gel electrophoresis (PAGE) under reducing conditions, with the exception of samples used to detect CD63, CD81 and CD9, and transferred on 0.22μm nitrocellulose membranes (BioRad). Membranes were blocked for 5 min at RT in EveryBlot Blocking Buffer (BioRad) and then incubated for 1 h at RT with different primary antibodies: mouse anti-CD63 (BD, #556019, 1:300), mouse anti-CD81 (BD, #555675, 1: 300), rabbit anti-CD9 (CST, #13403, 1:300), polyclonal anti-Alix (Invitrogen, #PA5-52873, 1:250), polyclonal anti-Syntenin 1 (Invitrogen, #PA5-92419, 1:200), mouse anti-Annexin 1 (BD, #610066, 1:200). Secondary antibodies horseradish peroxidase (HRP)-conjugated were used 1:3000 for 1 h at RT in EveryBlot. Western Blots were developed using Clarity Western ECL Substrate (BioRad). The presented immunoblots are representative of at least 3 independent experiments. Band analysis was performed using ImageLab software from BioRad.

5.11 Electron Microscopy

Transmission Electron Microscopy (TEM)

Negative staining was performed as described previously (Federici et al., 2020). Briefly, Bodipy sEV (>10^9 before and >10^7 after sorting as measured by NTA), were suspended in PBS (100 μl) and 10 μl were adsorbed on formvar-carbon coated grids. Ammonium molybdate 4% pH 6.4 (5 μl) was added as contrasting solution for 30

seconds and adsorbed with filter paper. Samples were air dried and observed by PHILIPS EM208S TEM (FEI, ThermoFisher).

Immuno-electron microscopy (Muhammad Zaeem Noman & Bassam Janji)

IEM was performed on the total sEV derived from Bodipy C16 pulsed cells, adsorbed on formvar-carbon coated grids. Samples were air-dried and transferred (membrane side down) to a drop of rabbit polyclonal anti-Bodipy (Invitrogen, #A-5770, 10 μg/ml;) or mouse monoclonal anti-CD81 (Santa Cruz Biotechnology, #sc-166029, 1:10) or mouse monoclonal anti-CD63 (BD, #556019, 5 μg/ml) in PBS for 1 h at RT, rinsed in buffer, incubated on 10 nm gold-conjugated goat anti-rabbit IgG (Sigma, #G3779, 1:30,) or 10 nm gold-conjugated goat anti-mouse IgG (Sigma, #G777, 1:30) in buffer for an additional h. Double immunolabeling was performed with anti-CD63 and anti-Bodipy antibodies, applied one by one. Anti-mouse IgG 10 nm and anti-rabbit IgG 5 nm gold-conjugated were chosen for showing anti-CD63 and anti-Bodipy antibody respectively. Samples were rinsed in buffer and successively incubated on a drop of 2% paraformaldehyde in PBS for 5 min. After a rapid final rinse with water, the grids were stained by ammonium molybdate as previously described and observed by a PHILIPS EM208S TEM (FEI, ThermoFisher).

Scanning Electron Microscopy (Ricklefs et al.)

SEM was performed as previously described (Federici et al., 2020). Bodipy sEV (before and after sorting, same amounts as above), were suspended in PBS (100 μl) and were left to adhere to polylisine treated round glass coverslips for 1 h. Samples were fixed with glutaraldehyde 2,5% in Na-cacodylate buffer 0,1M for 1 h and processed for SEM. Briefly, samples were post fixed with 1% OsO_4 in 0.1 M sodium cacodylate buffer 0,1M for 1h at RT and were dehydrated through a graded series of ethanol solutions (from 30% to 100%). Then, absolute ethanol was gradually substituted by a 1:1 solution of hexamethyldisilazane (HMDS) and absolute ethanol for 30 min, and successively by pure HMDS for 1 hr at RT. The final drying process

was concluded removing completely the HMDS and leaving to evaporate all the liquid phase on air, drying the samples at RT for 2 h and in a desiccator o.n. Finally, samples were mounted on stubs, lightly gold sputtered and analyzed in a field emission GeminiSEM450 (ZEISS). High magnification TEM images of total sEV or Bodipy-sorted sEV were analyzed by Fiji, Image J open source (Schindelin et al., 2012) and vesicles more than 30 nm in diameter were taken into account for collecting manual measures (N>100).

5.12 Analysis of the colocalization of Bodipy exo with exosomal markers

Bodipy exo isolated by ultracentrifugation were incubated with 5 μl of anti-CD63 BV421 antibody (BD, #740080), 10 μl of anti-CD81 APC antibody (BD, #551112), and 5 μl of anti-CD9 PE antibody (BD, #555372) to determine colocalization between Bodipy exo and the tetraspanins. As negative controls Bodipy exo were incubated with isotype antibody IgG1,κ conjugated to BV421 (Biolegend,#400157), APC (BD, #555751), or PE (BD, #555749) for 45 min at RT in a HulaMixer Sample Mixer in PBS with 2% FBS. Sample were fixed with 4% PFA for 30 min at RT, and then samples were washed with PBS at 500 x g for 20 min at 4°C. The supernatant was discarded, and vesicles were resuspended in PBS the colocalization percentage of Bodipy C16 with anti-CD63-BV421, anti-CD81-APC, and anti-CD9-PE was then determined by flow cytometry.

5.13 Bodipy exo glycosylation analysis

To study glycoylation of Bodipy exo, they have been incubated with 50 μg/ml of Concanavalin A coniugated with Alexa Fluor 647 (Con A) (Thermo Fisher, #C21421). For 45 min at RT. 4% PFA was added for 30 minutes at RT, then Bodipy exo were washed at 500xg for 20 min at 4°C. The glycosylation profile was analyzed by FC.

5.14 Generation of immature dendrtitic cells from PBMC

Peripheral blood mononuclear cells (PBMCs) were isolated from healthy donors buffy-coats by Ficoll-Paque (Sigma, #17-1440-02) density centrifugation. CD14+ monocyte population was purified by positive immunomagnetic bead selection (130-097-052, Miltenyi Biotec), according to the manufacturer's instructions. Freshly isolated monocyte were resuspended in RPMI 1640 medium supplemented with 200 mM glutamine, 100mg / ml streptomycin and 100 U/ml penicillin and 10% ultralow endotoxin fetal bovine serum (FBS) (Avantor, #97068-085), in the presence of GM-CSF (50 ng/mL) (130-093-865,Mylteni Biotec) and IL-4 (20 ng/mL) (130-093-922,Mylteni Biotec) to generate immature dendritic cells (iDCs). Cells were cultured at 37 °C, in a 5% CO2 and 95% H2O atmosphere. After 6 days, iDCs have been analyzed by FC for typical markers: CD14 PE (BioLegend, #367104,), CD1a BB700 (BD746202, BD), CD80 APC (BioLegend, #305220,), CD86 PE/Cy7 (BioLegend, #374210) , CD83 BV421 (BioLegend, #305324), CD206 APC/Cy7 (BioLegend, #321120), CD209 FITC (BioLegend, #330104), CD11c BUV661 (BD,#12968), HLA-DR PE-CF594 (BD, #562331), HLA-A2 Super Bright 600 (eBioscience, #63-9876-41). Negative control was set on correspective isotype.

5.15 Transfer of Bodipy exo to immature dendritic cells

iDCs cells were plated in 96-well plates and incubated with increasing numbers of Bodipy exo secreted from A375/M cells. To inhibit uptake via CD206 or MR mannose receptor, was used as competitor the y. mannan 2 mg/ml (Sigma, #M-7504). The uptake was performed for 30 minutes at 37°C in Hank's Balanced Salt Solution. Cells were then analyzed by FC in the presence of the vital dye TO-PRO3 iodide (Thermo Fisher, #T3605). Through a MESF curve (Molecules of a soluble fluorochrome equivalent) (Bang Laboratories, #555B) and a specific table supplied with the kit, it is possible to transform the FITC signal emitted by the Bodipy exo and by cells into a quantum of fluorescein. By comparing the amount of fluorescein in the sEV to that of the cell, it is possible to quantify the sEV transferred within the latter. As negative

control, cells not incubated with sEV were also analyzed. iDCs were cultured in presence of LPS, normoxic or hypoxic sEV for 48 h in presence or absence of y.mannan and the expression level of TNF-α and IL-12p70 in culture medium were determined by using a DuoSet ELISA assay kit (R&D systems) following manufacturer's instructions.

5.16 Statistical Analysis

Statistical analyses in this study were conducted with Graphpad Prism 9.5 software. The data are presented as the mean ± SEM from at least 3 independent experiments. Individual group statistical comparisons were analyzed by the two-tailed Student t test. A p-value < 0.05 (two-sided) was considered statistically significant.

6. References

Aheget, H., Tristan-Manzano, M., Mazini, L., Cortijo-Gutierrez, M., Galindo-Moreno, P., Herrera, C., Benabdellah, K. (2020). Exosome: A New Player in Translational Nanomedicine. *J Clin Med, 9*(8). doi: 10.3390/jcm9082380

Akoumi, A., Haffar, T., Mousterji, M., Kiss, R. S., & Bousette, N. (2017). Palmitate mediated diacylglycerol accumulation causes endoplasmic reticulum stress, Plin2 degradation, and cell death in H9C2 cardiomyoblasts. *Experimental Cell Research, 354*(2), 85-94. doi: 10.1016/j.yexcr.2017.03.032

Amanda P.B. Albuquerque1, M. B., Stefan Mereiter, Filipe Pinto, Celso, & A. Reis, a. E. I. C. B. (2018). Hypoxia and serum deprivation induces glycan alterations in triple negative breast cancer cells. doi: 10.1515/hsz-2018-0121

Amber, G., Ron, M., Janviere, K., Paul, A. V., & Nathan, R. W. (2019). Cellular-Defined Microenvironmental Internalization of Exosomes. In B. Ana Gil De & C. Jose Antonio Reales (Eds.), *Extracellular Vesicles and Their Importance in Human Health* (pp. Ch. 3). Rijeka: IntechOpen.

Andres, A., Fiorella, K., Gamelas, M. J., & Sebastian, A. (2016). Dendritic cell maturation and cross-presentation timing matters. *Immunological Reviews, 272*.

Anneke J. Engering, M. C., Fluitsma, D. M., & Elisabeth C. M. Hoefsmit, A. L., and Jean Pieters. (1997). MANNOSE RECEPTOR MEDIATED ANTIGEN UPTAKE AND PRESENTATION IN HUMAN DENDRITIC CELLS.

Ariel, S., & Sebastian, A. (2007). Phagocytosis and antigen presentation in dendritic cells. *Immunological Reviews, 219*.

Arneth, B. (2019). Tumor Microenvironment. *Medicina (Kaunas), 56*(1). doi: 10.3390/medicina56010015

Banerjee, S., Cui, H., Xie, N., Tan, Z., Yang, S., Icyuz, M., Liu, G. (2013). miR-125a-5p regulates differential activation of macrophages and inflammation. *J Biol Chem, 288*(49), 35428-35436. doi: 10.1074/jbc.M112.426866

Barutta, F., Corbetta, B., Bellini, S., Guarrera, S., Matullo, G., Scandella, M., Gruden, G. (2021). MicroRNA 146a is associated with diabetic complications in type 1 diabetic patients from the EURODIAB PCS. *J Transl Med, 19*(1), 475. doi: 10.1186/s12967-021-03142-4

Battistelli, M., & Falcieri, E. (2020). Apoptotic Bodies: Particular Extracellular Vesicles Involved in Intercellular Communication. *Biology (Basel), 9*(1). doi: 10.3390/biology9010021

Boussadia, Z., Lamberti, J., Mattei, F., Pizzi, E., Puglisi, R., Zanetti, C., Parolini, I. (2018). Acidic microenvironment plays a key role in human melanoma progression through a sustained exosome mediated transfer of clinically relevant metastatic molecules. *J Exp Clin Cancer Res, 37*(1), 245. doi: 10.1186/s13046-018-0915-z

Burgdorf, S., Kautz, A., Bohnert, V., Knolle, P. A., & Kurts, C. (2007). Distinct pathways of antigen uptake and intracellular routing in CD4 and CD8 T cell activation. *Science, 316*(5824), 612-616. doi: 10.1126/science.1137971

Burgdorf, S., & Kurts, C. (2008). Endocytosis mechanisms and the cell biology of antigen presentation. *Curr Opin Immunol, 20*(1), 89-95. doi: 10.1016/j.coi.2007.12.002

Burgdorf, S., Lukacs-Kornek, V., & Kurts, C. (2006). The mannose receptor mediates uptake of soluble but not of cell-associated antigen for cross-presentation. *J Immunol, 176*(11), 6770-6776. doi: 10.4049/jimmunol.176.11.6770

Chang, L. C., Chiu, H. M., Wu, M. S., & Shen, T. L. (2022). The Role of Small Extracellular Vesicles in the Progression of Colorectal Cancer and Its Clinical Applications. *Int J Mol Sci, 23*(3). doi: 10.3390/ijms23031379

Clancy, J. W., Schmidtmann, M., & D'Souza-Schorey, C. (2021). The ins and outs of microvesicles. *FASEB Bioadv, 3*(6), 399-406. doi: 10.1096/fba.2020-00127

Colombo, M., Raposo, G., & Thery, C. (2014). Biogenesis, secretion, and intercellular interactions of exosomes and other extracellular vesicles. *Annu Rev Cell Dev Biol, 30*, 255-289. doi: 10.1146/annurev-cellbio-101512-122326

Coscia, C., Parolini, I., Sanchez, M., Biffoni, M., Boussadia, Z., Zanetti, C., Sargiacomo, M. (2016). Generation, Quantification, and Tracing of Metabolically Labeled Fluorescent Exosomes. *Methods Mol Biol, 1448*, 217-235. doi: 10.1007/978-1-4939-3753-0_16

Dixson, A. C., Dawson, T. R., Di Vizio, D., & Weaver, A. M. (2023). Context-specific regulation of extracellular vesicle biogenesis and cargo selection. *Nat Rev Mol Cell Biol, 24*(7), 454-476. doi: 10.1038/s41580-023-00576-0

Echevarria, J., Royo, F., Pazos, R., Salazar, L., Falcon-Perez, J. M., & Reichardt, N. C. (2014). Microarray-based identification of lectins for the purification of human urinary extracellular vesicles directly from urine samples. *Chembiochem, 15*(11), 1621-1626. doi: 10.1002/cbic.201402058

Escola, J. M., Kleijmeer, M. J., Stoorvogel, W., Griffith, J. M., Yoshie, O., & Geuze, H. J. (1998). Selective enrichment of tetraspan proteins on the internal vesicles of multivesicular endosomes and on exosomes secreted by human B-lymphocytes. *J Biol Chem, 273*(32), 20121-20127. doi: 10.1074/jbc.273.32.20121

Ezekowitzt, P. D. S. a. R. A. B. (1998). The mannose receptor is a pattern recognition receptor involved in host defense. *Philip D Stahl and R Alan B Ezekowitzt*.

Felicetti, F., Errico, M. C., Bottero, L., Segnalini, P., Stoppacciaro, A., Biffoni, M., Care, A. (2008). The promyelocytic leukemia zinc finger-microRNA-221/-222 pathway controls melanoma progression through multiple oncogenic mechanisms. *Cancer Res, 68*(8), 2745-2754. doi: 10.1158/0008-5472.CAN-07-2538

Fiani, M. L., Barreca, V., Sargiacomo, M., Ferrantelli, F., Manfredi, F., & Federico, M. (2020). Exploiting Manipulated Small Extracellular Vesicles to Subvert Immunosuppression at the Tumor Microenvironment through Mannose Receptor/CD206 Targeting. *Int J Mol Sci, 21*(17). doi: 10.3390/ijms21176318

Folch, J., Lees, M., & Stanley, G. H. S. (1957). A Simple Method for the Isolation and Purification of Total Lipides from Animal Tissues. *Journal of Biological Chemistry, 226*(1), 497-509. doi: 10.1016/s0021-9258(18)64849-5

Fordjour, F. K., Guo, C., Ai, Y., Daaboul, G. G., & Gould, S. J. (2022). A shared, stochastic pathway mediates exosome protein budding along plasma and endosome membranes. *J Biol Chem, 298*(10), 102394. doi: 10.1016/j.jbc.2022.102394

Gazi, U., & Martinez-Pomares, L. (2009). Influence of the mannose receptor in host immune responses. *Immunobiology, 214*(7), 554-561. doi: 10.1016/j.imbio.2008.11.004

Gerlach, J. Q., & Griffin, M. D. (2016). Getting to know the extracellular vesicle glycome. *Mol Biosyst, 12*(4), 1071-1081. doi: 10.1039/c5mb00835b

Gonda, A., Kabagwira, J., Senthil, G. N., & Wall, N. R. (2019). Internalization of Exosomes through Receptor-Mediated Endocytosis. *Mol Cancer Res, 17*(2), 337-347. doi: 10.1158/1541-7786.MCR-18-0891

Griffiths, G., Gruenberg, J., Marsh, M., Wohlmann, J., Jones, A. T., & Parton, R. G. (2022). Nanoparticle entry into cells; the cell biology weak link. *Adv Drug Deliv Rev, 188*, 114403. doi: 10.1016/j.addr.2022.114403

Groot Kormelink, T., Arkesteijn, G. J., Nauwelaers, F. A., van den Engh, G., Nolte-'t Hoen, E. N., & Wauben, M. H. (2016). Prerequisites for the analysis and sorting of extracellular vesicle subpopulations by high-resolution flow cytometry. *Cytometry A, 89*(2), 135-147. doi: 10.1002/cyto.a.22644

Gurung, S., Perocheau, D., Touramanidou, L., & Baruteau, J. (2021). The exosome journey: from biogenesis to uptake and intracellular signalling. *Cell Commun Signal, 19*(1), 47. doi: 10.1186/s12964-021-00730-1

Han, L., Xu, J., Xu, Q., Zhang, B., Lam, E. W., & Sun, Y. (2017). Extracellular vesicles in the tumor microenvironment: Therapeutic resistance, clinical biomarkers, and targeting strategies. *Med Res Rev, 37*(6), 1318-1349. doi: 10.1002/med.21453

Harris, A. L. (2002). Hypoxia--a key regulatory factor in tumour growth. *Nat Rev Cancer, 2*(1), 38-47. doi: 10.1038/nrc704

He, G., Peng, X., Wei, S., Yang, S., Li, X., Huang, M., Li, H. (2022). Exosomes in the hypoxic TME: from release, uptake and biofunctions to clinical applications. *Mol Cancer, 21*(1), 19. doi: 10.1186/s12943-021-01440-5

Higginbotham, J. N., Zhang, Q., Jeppesen, D. K., Scott, A. M., Manning, H. C., Ochieng, J., . . . Coffey, R. J. (2016). Identification and characterization of EGF receptor in individual exosomes by fluorescence-activated vesicle sorting. *J Extracell Vesicles, 5*, 29254. doi: 10.3402/jev.v5.29254

Hoshino, A., Kim, H. S., Bojmar, L., Gyan, K. E., Cioffi, M., Hernandez, J., .Lyden, D. (2020). Extracellular Vesicle and Particle Biomarkers Define Multiple Human Cancers. *Cell, 182*(4), 1044-1061 e1018. doi: 10.1016/j.cell.2020.07.009

Hu, C., Chen, M., Jiang, R., Guo, Y., Wu, M., & Zhang, X. (2018). Exosome-related tumor microenvironment. *J Cancer, 9*(17), 3084-3092. doi: 10.7150/jca.26422

Hurwitz, S. N., Conlon, M. M., Rider, M. A., Brownstein, N. C., & Meckes, D. G., Jr. (2016). Nanoparticle analysis sheds budding insights into genetic drivers of extracellular vesicle biogenesis. *J Extracell Vesicles, 5*, 31295. doi: 10.3402/jev.v5.31295

Inglis, H. C., Danesh, A., Shah, A., Lacroix, J., Spinella, P. C., & Norris, P. J. (2015). Techniques to improve detection and analysis of extracellular vesicles using flow cytometry. *Cytometry A, 87*(11), 1052-1063. doi: 10.1002/cyto.a.22649

Jeppesen, D. K., Fenix, A. M., Franklin, J. L., Higginbotham, J. N., Zhang, Q., Zimmerman, L. J., Coffey, R. J. (2019). Reassessment of Exosome Composition. *Cell, 177*(2), 428-445 e418. doi: 10.1016/j.cell.2019.02.029

Jing, X., Yang, F., Shao, C., Wei, K., Xie, M., Shen, H., & Shu, Y. (2019). Role of hypoxia in cancer therapy by regulating the tumor microenvironment. *Mol Cancer, 18*(1), 157. doi: 10.1186/s12943-019-1089-9

Kalluri, R. (2016). The biology and function of exosomes in cancer. *J Clin Invest, 126*(4), 1208-1215. doi: 10.1172/JCI81135

Kalluri, R., & LeBleu, V. S. (2020). The biology, function, and biomedical applications of exosomes. *Science, 367*(6478). doi: 10.1126/science.aau6977

Kalra, H., Drummen, G. P., & Mathivanan, S. (2016). Focus on Extracellular Vesicles: Introducing the Next Small Big Thing. *Int J Mol Sci, 17*(2), 170. doi: 10.3390/ijms17020170

Karimi, N., Dalirfardouei, R., Dias, T., Lotvall, J., & Lasser, C. (2022). Tetraspanins distinguish separate extracellular vesicle subpopulations in human serum and plasma - Contributions of platelet extracellular vesicles in plasma samples. *J Extracell Vesicles, 11*(5), e12213. doi: 10.1002/jev2.12213

Khan, N. A., Asim, M., Biswas, K. H., Alansari, A. N., Saman, H., Sarwar, M. Z., Uddin, S. (2023). Exosome nanovesicles as potential biomarkers and immune checkpoint signaling modulators in lung cancer microenvironment: recent advances and emerging concepts. *J Exp Clin Cancer Res, 42*(1), 221. doi: 10.1186/s13046-023-02753-7

Kondo, K., Harada, Y., Nakano, M., Suzuki, T., Fukushige, T., Hanzawa, K., . . . Inoue, H. (2022). Identification of distinct N-glycosylation patterns on extracellular vesicles from small-cell and non-small-cell lung cancer cells. *J Biol Chem, 298*(6), 101950. doi: 10.1016/j.jbc.2022.101950

Kowal, J., Arras, G., Colombo, M., Jouve, M., Morath, J. P., Primdal-Bengtson, B., . . . Thery, C. (2016). Proteomic comparison defines novel markers to characterize heterogeneous populations of extracellular vesicle subtypes. *Proc Natl Acad Sci U S A, 113*(8), E968-977. doi: 10.1073/pnas.1521230113

Kreer, C., Rauen, J., Zehner, M., & Burgdorf, S. (2011). Cross-presentation: how to get there - or how to get the ER. *Front Immunol, 2*, 87. doi: 10.3389/fimmu.2011.00087

Krishnamoorthy, L., Bess, J. W., Jr., Preston, A. B., Nagashima, K., & Mahal, L. K. (2009). HIV-1 and microvesicles from T cells share a common glycome, arguing for a common origin. *Nat Chem Biol, 5*(4), 244-250. doi: 10.1038/nchembio.151

Kuhn, D. A., Vanhecke, D., Michen, B., Blank, F., Gehr, P., Petri-Fink, A., & Rothen-Rutishauser, B. (2014). Different endocytotic uptake mechanisms for nanoparticles in epithelial cells and macrophages. *Beilstein J Nanotechnol, 5*, 1625-1636. doi: 10.3762/bjnano.5.174

Lai, C. P., Kim, E. Y., Badr, C. E., Weissleder, R., Mempel, T. R., Tannous, B. A., & Breakefield, X. O. (2015). Visualization and tracking of tumour extracellular vesicle delivery and RNA translation using multiplexed reporters. *Nat Commun, 6*, 7029. doi: 10.1038/ncomms8029

Laoui, D., Movahedi, K., Van Overmeire, E., Van den Bossche, J., Schouppe, E., Mommer, C., Van Ginderachter, J. A. (2011). Tumor-associated macrophages in breast cancer: distinct subsets, distinct functions. *Int J Dev Biol, 55*(7-9), 861-867. doi: 10.1387/ijdb.113371dl

Larios, J., Mercier, V., Roux, A., & Gruenberg, J. (2020). ALIX- and ESCRT-III-dependent sorting of tetraspanins to exosomes. *J Cell Biol, 219*(3). doi: 10.1083/jcb.201904113

Lee, K., Fraser, K., Ghaddar, B., Yang, K., Kim, E., Balaj, L., Weissleder, R. (2018). Multiplexed Profiling of Single Extracellular Vesicles. *ACS Nano, 12*(1), 494-503. doi: 10.1021/acsnano.7b07060

Lee, R. T., Hsu, T. L., Huang, S. K., Hsieh, S. L., Wong, C. H., & Lee, Y. C. (2011). Survey of immune-related, mannose/fucose-binding C-type lectin receptors reveals widely divergent sugar-binding specificities. *Glycobiology, 21*(4), 512-520. doi: 10.1093/glycob/cwq193

Lee, Y. S., Kim, S. Y., Ko, E., Lee, J. H., Yi, H. S., Yoo, Y. J., Byun, K. S. (2017). Exosomes derived from palmitic acid-treated hepatocytes induce fibrotic activation of hepatic stellate cells. *Sci Rep, 7*(1), 3710. doi: 10.1038/s41598-017-03389-2

Li, I., & Nabet, B. Y. (2019). Exosomes in the tumor microenvironment as mediators of cancer therapy resistance. *Mol Cancer, 18*(1), 32. doi: 10.1186/s12943-019-0975-5

Lin, S., Zhou, S., & Yuan, T. (2020). The "sugar-coated bullets" of cancer: Tumor-derived exosome surface glycosylation from basic knowledge to applications. *Clin Transl Med, 10*(6), e204. doi: 10.1002/ctm2.204

Liu, D. R., Guan, Q. L., Gao, M. T., Jiang, L., & Kang, H. X. (2017). Mannose receptor as a potential biomarker for gastric cancer: a pilot study. *Int J Biol Markers, 32*(3), e278-e283. doi: 10.5301/jbm.5000244

Louie, S. M., Roberts, L. S., Mulvihill, M. M., Luo, K., & Nomura, D. K. (2013). Cancer cells incorporate and remodel exogenous palmitate into structural and oncogenic signaling lipids. *Biochim Biophys Acta, 1831*(10), 1566-1572. doi: 10.1016/j.bbalip.2013.07.008

Lucchetti, D., Colella, F., Perelli, L., Ricciardi-Tenore, C., Calapa, F., Fiori, M. E., Sgambato, A. (2020). CD147 Promotes Cell Small Extracellular Vesicles Release during Colon Cancer Stem Cells Differentiation and Triggers Cellular Changes in Recipient Cells. *Cancers (Basel), 12*(2). doi: 10.3390/cancers12020260

Malhi, H., Bronk, S. F., Werneburg, N. W., & Gores, G. J. (2006). Free fatty acids induce JNK-dependent hepatocyte lipoapoptosis. *J Biol Chem, 281*(17), 12093-12101. doi: 10.1074/jbc.M510660200

Mantovani, A., & Allavena, P. (2015). The interaction of anticancer therapies with tumor-associated macrophages. *J Exp Med, 212*(4), 435-445. doi: 10.1084/jem.20150295

Mantovani, A., Marchesi, F., Malesci, A., Laghi, L., & Allavena, P. (2017). Tumour-associated macrophages as treatment targets in oncology. *Nat Rev Clin Oncol, 14*(7), 399-416. doi: 10.1038/nrclinonc.2016.217

Martinez-Pomares, L. (2012). The mannose receptor. *J Leukoc Biol, 92*(6), 1177-1186. doi: 10.1189/jlb.0512231

Martinez-Pomares, L., Mantovani, G., & Stahl, P. D. (2023). The Mannose Receptor (CD206) and Its Siblings-The Back Story. 525-542. doi: 10.1016/b978-0-12-821618-7.00234-0

Martins, A. M., Ramos, C. C., Freitas, D., & Reis, C. A. (2021). Glycosylation of Cancer Extracellular Vesicles: Capture Strategies, Functional Roles and Potential Clinical Applications. *Cells, 10*(1). doi: 10.3390/cells10010109

Mathieu, M., Martin-Jaular, L., Lavieu, G., & Thery, C. (2019). Specificities of secretion and uptake of exosomes and other extracellular vesicles for cell-to-cell communication. *Nat Cell Biol, 21*(1), 9-17. doi: 10.1038/s41556-018-0250-9

Mathieu, M., Nevo, N., Jouve, M., Valenzuela, J. I., Maurin, M., Verweij, F. J., Thery, C. (2021). Specificities of exosome versus small ectosome secretion revealed by live intracellular tracking of CD63 and CD9. *Nat Commun, 12*(1), 4389. doi: 10.1038/s41467-021-24384-2

McKelvey, K. J., Powell, K. L., Ashton, A. W., Morris, J. M., & McCracken, S. A. (2015). Exosomes: Mechanisms of Uptake. *J Circ Biomark, 4*, 7. doi: 10.5772/61186

Meckes, D. G., Jr., Gunawardena, H. P., Dekroon, R. M., Heaton, P. R., Edwards, R. H., Ozgur, S., . . . Raab-Traub, N. (2013). Modulation of B-cell exosome proteins by gamma herpesvirus infection. *Proc Natl Acad Sci U S A, 110*(31), E2925-2933. doi: 10.1073/pnas.1303906110

Meldolesi, J. (2022). Unconventional Protein Secretion Dependent on Two Extracellular Vesicles: Exosomes and Ectosomes. *Front Cell Dev Biol, 10*, 877344. doi: 10.3389/fcell.2022.877344

Montecalvo, A., Shufesky, W. J., Stolz, D. B., Sullivan, M. G., Wang, Z., Divito, S. J., Morelli, A. E. (2008). Exosomes as a short-range mechanism to spread alloantigen between dendritic cells during T cell allorecognition. *J Immunol, 180*(5), 3081-3090. doi: 10.4049/jimmunol.180.5.3081

Morales-Kastresana, A., Musich, T. A., Welsh, J. A., Telford, W., Demberg, T., Wood, J. C. S., . . . Jones, J. C. (2019). High-fidelity detection and sorting of nanoscale vesicles in viral disease and cancer. *J Extracell Vesicles, 8*(1), 1597603. doi: 10.1080/20013078.2019.1597603

Morales-Kastresana, A., Telford, B., Musich, T. A., McKinnon, K., Clayborne, C., Braig, Z., . . . Jones, J. C. (2017). Labeling Extracellular Vesicles for Nanoscale Flow Cytometry. *Sci Rep, 7*(1), 1878. doi: 10.1038/s41598-017-01731-2

Mori, Y., Koike, M., Moriishi, E., Kawabata, A., Tang, H., Oyaizu, H., Yamanishi, K. (2008). Human herpesvirus-6 induces MVB formation, and virus egress occurs by an exosomal release pathway. *Traffic, 9*(10), 1728-1742. doi: 10.1111/j.1600-0854.2008.00796.x

Muhammad Zaeem Noman, M. H., Yosra Messai, Stéphane Terry, Claudine Kieda,, & Bassam Janji, a. S. C. (2015). Hypoxia: a key player in antitumor immune response. A Review in the

Theme: Cellular Responses to Hypoxia. *Am J Physiol Cell Physiol*. doi: 10.1152/ajpcell.00207.2015

Mulcahy, L. A., Pink, R. C., & Carter, D. R. (2014). Routes and mechanisms of extracellular vesicle uptake. *J Extracell Vesicles, 3*. doi: 10.3402/jev.v3.24641

Nail, H. M., Chiu, C. C., Leung, C. H., Ahmed, M. M. M., & Wang, H. D. (2023). Exosomal miRNA-mediated intercellular communications and immunomodulatory effects in tumor microenvironments. *J Biomed Sci, 30*(1), 69. doi: 10.1186/s12929-023-00964-w

Nieuwland, R., Falcon-Perez, J. M., Thery, C., & Witwer, K. W. (2020). Rigor and standardization of extracellular vesicle research: Paving the road towards robustness. *J Extracell Vesicles, 10*(2), e12037. doi: 10.1002/jev2.12037

Nyberg, P., Salo, T., & Kalluri, R. (2008). Tumor microenvironment and angiogenesis. *Front Biosci, 13*(7), 6537-6553.

Olzmann, J. A., & Carvalho, P. (2019). Dynamics and functions of lipid droplets. *Nat Rev Mol Cell Biol, 20*(3), 137-155. doi: 10.1038/s41580-018-0085-z

Paskeh, M. D. A., Entezari, M., Mirzaei, S., Zabolian, A., Saleki, H., Naghdi, M. J., . . . Ashrafizadeh, M. (2022). Emerging role of exosomes in cancer progression and tumor microenvironment remodeling. *J Hematol Oncol, 15*(1), 83. doi: 10.1186/s13045-022-01305-4

Penke, M., Schuster, S., Gorski, T., Gebhardt, R., Kiess, W., & Garten, A. (2017). Oleate ameliorates palmitate-induced reduction of NAMPT activity and NAD levels in primary human hepatocytes and hepatocarcinoma cells. *Lipids Health Dis, 16*(1), 191. doi: 10.1186/s12944-017-0583-6

Philip Stahl, P. H. S., Elaine Sigardson, Jane S. Rodman, Y.C. Lee (1980). Receptor-Mediated Pinocytosis of Mannose Glycoconjugates by Macrophages: Characterization and Evidence for Receptor Recycling *Cell, 19*(1), 207-215. doi: https://doi.org/10.1016/0092-8674(80)90402-X

Pol, A., Gross, S. P., & Parton, R. G. (2014). Review: biogenesis of the multifunctional lipid droplet: lipids, proteins, and sites. *J Cell Biol, 204*(5), 635-646. doi: 10.1083/jcb.201311051

Pospichalova, V., Svoboda, J., Dave, Z., Kotrbova, A., Kaiser, K., Klemova, D., Bryja, V. (2015). Simplified protocol for flow cytometry analysis of fluorescently labeled exosomes and microvesicles using dedicated flow cytometer. *J Extracell Vesicles, 4*, 25530. doi: 10.3402/jev.v4.25530

Ren, W., Hou, J., Yang, C., Wang, H., Wu, S., Wu, Y.,Lu, C. (2019). Extracellular vesicles secreted by hypoxia pre-challenged mesenchymal stem cells promote non-small cell lung cancer cell growth and mobility as well as macrophage M2 polarization via miR-21-5p delivery. *J Exp Clin Cancer Res, 38*(1), 62. doi: 10.1186/s13046-019-1027-0

Ricklefs, F. L., Maire, C. L., Reimer, R., Duhrsen, L., Kolbe, K., Holz, M., Lamszus, K. (2019). Imaging flow cytometry facilitates multiparametric characterization of extracellular vesicles in malignant brain tumours. *J Extracell Vesicles, 8*(1), 1588555. doi: 10.1080/20013078.2019.1588555

Robinson, M. J., Sancho, D., Slack, E. C., LeibundGut-Landmann, S., & Reis e Sousa, C. (2006). Myeloid C-type lectins in innate immunity. *Nat Immunol, 7*(12), 1258-1265. doi: 10.1038/ni1417

Rotsch, C., & Radmacher, M. (2000). Drug-induced changes of cytoskeletal structure and mechanics in fibroblasts: an atomic force microscopy study. *Biophysical Journal, 78*(0006-3495 (Print)).

Ruan, K., Song, G., & Ouyang, G. (2009). Role of hypoxia in the hallmarks of human cancer. *J Cell Biochem, 107*(6), 1053-1062. doi: 10.1002/jcb.22214

Ryan P. McNamara, B. A. D., Lindsey M. Costantini, Andrew G. MacLean, T. Alix Myers, Blake Schouest,Nicholas J. Maness, Jack D. Griffith, Blossom A. Damania, Andrew G. MacLean, Dirk P. Dittmera. (2021). Nef Secretion into Extracellular Vesicles or Exosomes Is Conserved across Human and Simian Immunodeficiency Viruses. *AmericanSociety for Microbiology*. doi: 10.1128/mBio.02344

Saba, R., Sorensen, D. L., & Booth, S. A. (2014). MicroRNA-146a: A Dominant, Negative Regulator of the Innate Immune Response. *Front Immunol, 5*, 578. doi: 10.3389/fimmu.2014.00578

Shimoda, A., Sawada, S. I., Sasaki, Y., & Akiyoshi, K. (2019). Exosome surface glycans reflect osteogenic differentiation of mesenchymal stem cells: Profiling by an evanescent field fluorescence-assisted lectin array system. *Sci Rep, 9*(1), 11497. doi: 10.1038/s41598-019-47760-x

Stahl, P. D., & Ezekowitz, R. A. (1998). The mannose receptor is a pattern recognition receptor involved in host defense. *Curr Opin Immunol.*(0952-7915 (Print)).

Surman, M., Hoja-Lukowicz, D., Szwed, S., Drozdz, A., Stepien, E., & Przybylo, M. (2018). Human melanoma-derived ectosomes are enriched with specific glycan epitopes. *Life Sci, 207*, 395-411. doi: 10.1016/j.lfs.2018.06.026

Taylor, P. R., Gordon, S., & Martinez-Pomares, L. (2005). The mannose receptor: linking homeostasis and immunity through sugar recognition. *Trends Immunol, 26*(2), 104-110. doi: 10.1016/j.it.2004.12.001

Teng, F., & Fussenegger, M. (2020). Shedding Light on Extracellular Vesicle Biogenesis and Bioengineering. *Adv Sci (Weinh), 8*(1), 2003505. doi: 10.1002/advs.202003505

Thomas, P., Arden, C., Corcoran, J., Hacker, C., Welters, H. J., & Morgan, N. G. (2022). Differential routing and disposition of the long-chain saturated fatty acid palmitate in rodent vs human beta-cells. *Nutr Diabetes, 12*(1), 22. doi: 10.1038/s41387-022-00199-y

Tran Janco, J. M., Lamichhane, P., Karyampudi, L., & Knutson, K. L. (2015). Tumor-infiltrating dendritic cells in cancer pathogenesis. *J Immunol, 194*(7), 2985-2991. doi: 10.4049/jimmunol.1403134

van der Zande, H. J. P., Nitsche, D., Schlautmann, L., Guigas, B., & Burgdorf, S. (2021). The Mannose Receptor: From Endocytic Receptor and Biomarker to Regulator of (Meta)Inflammation. *Front Immunol, 12*, 765034. doi: 10.3389/fimmu.2021.765034

van Niel, G., Carter, D. R. F., Clayton, A., Lambert, D. W., Raposo, G., & Vader, P. (2022). Challenges and directions in studying cell-cell communication by extracellular vesicles. *Nat Rev Mol Cell Biol, 23*(5), 369-382. doi: 10.1038/s41580-022-00460-3

van Niel, G., D'Angelo, G., & Raposo, G. (2018). Shedding light on the cell biology of extracellular vesicles. *Nat Rev Mol Cell Biol, 19*(4), 213-228. doi: 10.1038/nrm.2017.125

Verweij, F. J., Balaj, L., Boulanger, C. M., Carter, D. R. F., Compeer, E. B., D'Angelo, G., . . . van Niel, G. (2021). The power of imaging to understand extracellular vesicle biology in vivo. *Nat Methods, 18*(9), 1013-1026. doi: 10.1038/s41592-021-01206-3

Wanderley, C. W., Colon, D. F., Luiz, J. P. M., Oliveira, F. F., Viacava, P. R., Leite, C. A., Cunha, F. Q. (2018). Paclitaxel Reduces Tumor Growth by Reprogramming Tumor-Associated Macrophages to an M1 Profile in a TLR4-Dependent Manner. *Cancer Res, 78*(20), 5891-5900. doi: 10.1158/0008-5472.CAN-17-3480

Whiteside, T. L. (2016). Tumor-Derived Exosomes and Their Role in Cancer Progression. *Adv Clin Chem, 74*, 103-141. doi: 10.1016/bs.acc.2015.12.005

Williams, C., Pazos, R., Royo, F., Gonzalez, E., Roura-Ferrer, M., Martinez, A., Falcon-Perez, J. M. (2019). Assessing the role of surface glycans of extracellular vesicles on cellular uptake. *Sci Rep, 9*(1), 11920. doi: 10.1038/s41598-019-48499-1

Williams, C., Royo, F., Aizpurua-Olaizola, O., Pazos, R., Boons, G. J., Reichardt, N. C., & Falcon-Perez, J. M. (2018). Glycosylation of extracellular vesicles: current knowledge, tools and clinical perspectives. *J Extracell Vesicles, 7*(1), 1442985. doi: 10.1080/20013078.2018.1442985

Willms, E., Cabanas, C., Mager, I., Wood, M. J. A., & Vader, P. (2018). Extracellular Vesicle Heterogeneity: Subpopulations, Isolation Techniques, and Diverse Functions in Cancer Progression. *Front Immunol, 9*, 738. doi: 10.3389/fimmu.2018.00738

Willms, E., Johansson, H. J., Mager, I., Lee, Y., Blomberg, K. E., Sadik, M., Vader, P. (2016). Cells release subpopulations of exosomes with distinct molecular and biological properties. *Sci Rep, 6*, 22519. doi: 10.1038/srep22519

Woud, W. W., van der Pol, E., Mul, E., Hoogduijn, M. J., Baan, C. C., Boer, K., & Merino, A. (2022). An imaging flow cytometry-based methodology for the analysis of single extracellular vesicles in unprocessed human plasma. *Commun Biol, 5*(1), 633. doi: 10.1038/s42003-022-03569-5

Zhang, H., Freitas, D., Kim, H. S., Fabijanic, K., Li, Z., Chen, H., Lyden, D. (2018). Identification of distinct nanoparticles and subsets of extracellular vesicles by asymmetric flow field-flow fractionation. *Nat Cell Biol, 20*(3), 332-343. doi: 10.1038/s41556-018-0040-4

Zou, W. (2005). Immunosuppressive networks in the tumour environment and their therapeutic relevance. *Nat Rev Cancer, 5*(4), 263-274. doi: 10.1038/nrc1586